tural examination of the cornea.[10,11] Only two studies have used IVCM to study the corneas of patients with PEX syndrome. Martone et al.[12] reported the findings in one case, and they reported that ICVM can detect hyperreflective deposits and dendritic cells infiltrating the basal epithelial cell layer. Fibrillar subepithelial structures were found, and the endothelial layer showed cellular anomalies. In a prospective observational case series, Sbeity et al.[13] used noncontact IVCM to detect XFM on the lens surfaces and corneal endothelia of PEX eyes and their fellow eyes.

Our study was the first to use IVCM to investigate cell densities in different layers of the cornea and to determine alterations of subbasal nerve density and tortuosity in PEX and PEX fellow eyes. Our results showed a significant decrease in the densities of the corneal endothelial cells in PEX eyes and their fellow eyes, which is in agreement with earlier observations by specular microscopy.[8,19,20] In addition, the clear confocal images allowed us to detect pleomorphisms and polymegethisms of the endothelial cells. All PEX eyes and 51.9% of PEX fellow eyes showed deposits of hyperreflective material in the endothelium, indicative of either pigment granules or XFM. In agreement with Sbeity et al.,[13] we believe that the pleomorphic and irregular deposits found on the corneal endothelium most likely represent XFM rather than pigment granules, which are round and uniform in size.[13] In addition, a number of patients who had no visible pigment keratoprecipitates on slit-lamp microscopy were found to have abundant large and irregular hyperreflective deposits on the endothelium in the confocal images.

PEX syndrome–associated corneal endotheliopathy has been suggested to be caused by one or a combination of the following alterations: hypoxic changes in the anterior chamber, accumulation of extracellular matrix, fibroblastic changes of the endothelium, and increased concentration of TGF-β.[1-3] Our confocal microscopic findings suggest that the XFM, possibly at different stages of the normal course of PEX, may be deposited on the endothelium or may migrate from the endothelial cells that undergo fibroblastic changes. Our findings also showed that hyperreflective materials are found not only on the endothelium of PEX eyes but also in their fellow eyes, indicating that the fellow eyes might be at a preclinical stage of PEX syndrome. A bilateral decrease in the endothelial cell counts and morphologic alterations of endothelium support the idea that PEX is a binocular and systemic abnormality. Patients with unilateral PEX syndrome may have asymmetric manifestation of this slowly progressing disease.

Of clinical significance was our finding that the decreased stromal cell densities observed by IVCM could possibly explain the report that the central corneas of PEX eyes were thinner than those of normal subjects.[8] The pathogenesis of the decrease of stromal cell density in PEX eyes warrants future study. Because XFM deposits were simultaneously observed in the anterior stroma of PEX eyes, we suggest that the XFM may be somehow causative for this alteration, perhaps by inducing apoptosis of the keratocytes. Other pathogenic factors, such as altered levels of cytokines or chemokines in the cornea, could also be responsible, and this definitely warrants future investigation. In addition, PEX fellow eyes also had lower cell counts in the stroma, although the difference was not statistically significant. We suggest that the cause of the binocular differences in our study might have been because the two eyes were at different stages of the PEX process, and PEX fellow eyes may still be at a preclinical stage of PEX syndrome.

Other important findings were found in the subbasal nerve plexus. Our results showed that the subbasal nerve density was significantly lower and the nerves were mostly tortuous, with beading and thinning in PEX eyes. Interestingly, PEX fellow eyes also had similar alterations, though the changes were not significant. These findings support the idea that PEX syndrome is a binocular abnormality that is expressed in both eyes but to different degrees. The important clinical significance of our study is that our correlation analyses showed that the decreased subbasal nerve density and increased tortuosity were significantly correlated with decreased corneal sensitivity. These results provide evidence, for the first time, that the cause of the decreased corneal sensitivity in eyes with PEX syndrome is the decreased subbasal nerve density. For patients with PEX syndrome, it would be practical and feasible to examine corneal sensitivity to assess the severity of PEX keratopathy and perhaps to predict the progression of PEX syndrome. In addition, detection of the morphologic changes in cell densities and subbasal nerve abnormalities by IVCM in the fellow eyes indicates that it is a sensitive tool for the diagnosis of preclinical stage of PEX syndrome. Our findings showed that PEX keratopathy may develop before any clinically visible XFM deposits are detected on the lens capsule or iris. If these findings are confirmed, then keratopathy may be the first event of the ocular complications of PEX syndrome. These findings also indicate that clinically unaffected fellow eyes of patients with PEX syndrome are probably at risk for PEX syndrome, and more frequent ophthalmologic examinations are necessary.

This study has increased our understanding of the keratopathy of this most likely systemic abnormality. Whether the alternations of the subbasal corneal nerves are primary or secondary changes of the disease must be determined. Because of the increase in the elastic microfibril components and imbalances in the matrix metalloproteinases (MMPs) and tissue inhibitors of MMP in eyes with PEX syndrome, PEX fibrils accumulate in the tissues.[1-3] Our findings that XFM deposits were frequently observed close to the subbasal epithelial layer or anterior stroma support the idea that besides an abnormal aggregation of elastic microfibrils into exfoliation fibers (the elastic microfibril hypothesis),[1-3,21] other extracellular matrix components, such as basement membrane components, may possibly interact and become incorporated into the composite XFM (the basement membrane hypothesis).[2,3] In addition, our observation of an infiltration of dendritic cells in close vicinity of the subbasal nerve plexus layer indicates the possibility that accumulation of extracellular XFM may induce inflammatory responses, which then recruit antigen-presenting cells such as immunocompetent dendritic cells. This excessive deposition of XFM and infiltration of dendritic cells may play a role in the neuropathy of the subbasal nerve plexus, resulting in decreased corneal sensitivity in patients with PEX syndrome.

Some limitations were present this study. First, the IVCM scans a very small area of the cornea, which may generate biases among different portions of scanning of different groups. As mentioned, efforts were taken to scan the center of the cornea of each subject. In addition, we also confirmed our findings by scanning the midperipheral and peripheral portions of the cornea (data not shown).

Second, IVCM images may not represent the true histologic changes of the cornea. By applying the same criteria for image evaluation, we can conclude that the differences between the studied groups were still detected. Furthermore, it was our impression that fewer keratocytes were seen in the stromas of corneal specimens obtained from PEX syndrome patients with penetrating keratoplasty.

Future investigations, including a thorough and quantitative analysis of the exfoliation material by confocal imaging, are needed. In addition, the correlations between IVCM findings with endothelial barrier function should be determined. If the confocal findings can provide clues for preclinical stages of endothelial barrier dysfunction of the cornea in PEX syndrome, their clinical significance can be used in designing an early treatment protocol.

In summary, our study demonstrated that eyes with PEX syndrome have decreased cell densities in the cornea. The subbasal nerve density was also significantly decreased, and this was significantly correlated with clinically decreased corneal sensitivity. Our study sheds light on understanding the cause of impaired corneal sensitivity in patients with PEX syndrome. The PEX syndrome is probably a bilateral event in which the keratopathy of the fellow eye also must be observed.

References

1. Naumann GOH, Schlötzer-Schrehardt U, Kuchle M. Pseudoexfoliation syndrome for the comprehensive ophthalmologist: intraocular and systemic manifestations. *Ophthalmology.* 1998;105:951-968.
2. Schlötzer-Schrehardt U, Naumann GOH. Ocular and systemic pseudoexfoliation syndrome. *Am J Ophthalmol.* 2006;141:921-937.
3. Ritch R, Schlötzer-Schrehardt U. Exfoliation syndrome. *Surv Ophthalmol.* 2001;45:265-315.
4. Forsius H. Prevalence of pseudoexfoliation of the lens in Finns, Lapps, Icelanders, Eskimos, and Russian. *Trans Ophthalmol Soc UK.* 1979;99:296-298.
5. Naumann GOH, Schlötzer-Schrehardt U. Keratopahty in pseudoexfoliation syndrome as a cause of corneal endothelial decompensation—a clinicopathologic study. *Ophthalmology.* 2000;107:1111-1124.
6. Abbott RL, Fine BS, Webster RB Jr, et al. Specular microscopic and histologic observations in nonguttata corneal endothelial degeneration. *Ophthalmology.* 1981;88:788-800.
7. Detorakis ET, Koukoula S, Chrisohoou F, Konstas AG, Kozobolis VP. Central corneal mechanical sensitivity in pseudoexfoliation syndrome. *Cornea.* 2005;24:688-691.
8. Inoue K, Okugawa K, Oshika T, Amano S. Morphological study of corneal endothelium and corneal thickness in pseudoexfoliation syndrome. *Jpn J Ophthalmol.* 2003;47:235-239.
9. Kozobolis VP, Christodoulakis EV, Naoumidi II, Siganos CS, Detorakis ET, Pallikaris LG. Study of conjunctival goblet cell morphology and tear film stability in pseudoexfoliation syndrome. *Graefes Arch Clin Exp Ophthalmol.* 2004;242:478-483.
10. Patel DV, McGhee CNJ. In vivo confocal microscopy of human corneal nerves in health, in ocular and systemic disease, and following corneal surgery: a review. *Br J Ophthalmol.* 2009;93:853-860.
11. Guthoff RF, Zhivov A, Stachs O. In vivo confocal microscopy, an inner vision of the cornea—a major review. *Clin Exp Ophthalmol.* 2009;37:100-117.
12. Martone G, Casprini F, Traaversi C, Lepri F, Picherri P, Caporossi A. Pseudoexfoliation syndrome: in vivo confocal microscopy analysis. *Clin Exp Ophthalmol.* 2007;35:582-585.
13. Sbeity Z, Palmiero PM, Tello C. Liebmann JM, Ritch R. Non-contact in vivo confocal scanning laser microscopy in exfoliation syndrome, exfoliation syndrome suspect and normal eyes. *Acta Ophthalmol.* 2009 Oct 23 [Epub ahead of print].
14. Hu Y, Matsumoto Y, Adan ES, et al. Corneal in vivo confocal scanning laser microscopy in patients with atopic keratoconjunctivitis. *Ophthalmology.* 2008;115:2004-2012.
15. Quadrado MJ, Popper M, Morgado AM, Murta JN, Best JAV. Diabetes and corneal cell densities in humans by in vivo confocal microscopy. *Cornea.* 2006;25:761-768.
16. Mocan MC, Durukan I, Irkec M, Orhan M. Morphologic alterations of both the stromal and subbasal nerves in the corneas of patients with diabetes. *Cornea.* 2006;25:769-773.
17. Schlötzer-Schrehardt U, Koca M, Naumann GOH, Volkholz H. Pseudoexfoliation syndrome: ocular manifestation of a systemic disorder? *Arch Ophthalmol.* 1992;110:1752-1756.
18. Thorleifsson G, Magnusson KP, Sulem P, et al. Common sequence variants in the LOXL1 gene confer susceptibility to exfoliation glaucoma. *Science.* 2007;317:1397-1400.
19. Wang L, Yamasita R, Hommura S. Corneal endothelial changes and aqueous flare intensity in pseudoexfoliation syndrome. *Ophthalmologica.* 1999;213:318-391.
20. Miyake K, Matsuda M, Inaba M. Corneal endothelial changes in pseudoexfoliation syndrome. *Am J Ophthalmol.* 1989;108:49-52.
21. Streeten BW, Gibson SA, Dark AJ. Pseudoexfoliative material contains an elastic microfibillar-associated glycoprotein. *Trans Am Ophthalmol Soc.* 1986;84:304-320.

Anterior Segment Optical Coherence Tomography Analysis of Clinically Unilateral Pseudoexfoliation Syndrome: Evidence of Bilateral Involvement and Morphologic Factors Related to Asymmetry

Xiaodong Zheng,[1] *Hiroshi Sakai,*[2] *Tomoko Goto,*[1,3] *Koji Namiguchi,*[1] *Shiro Mizoue,*[1] *Atsushi Shiraishi,*[1] *Shoichi Sawaguchi,*[2] *and Yuichi Ohashi*[1]

Purpose. To compare the morphology of the anterior chamber angle (ACA) and iris in eyes with pseudoexfoliation (PEX) syndrome to that of their clinically unaffected fellow eyes and normal control eyes.

Methods. Forty-two patients with unilateral PEX syndrome and 42 normal subjects were studied. Eyes were separated into those with PEX, their clinically unaffected fellow eyes, and normal eyes. The dark-light changes of the ACA and iris were documented by anterior segment optical coherence tomography (AS-OCT) video recordings. The nasal ACA parameters including the angle opening distance at 500 μm (AOD500), the trabecular-iris space at 500 μm (TISA500), and the trabecular-iris angle at 500 μm (TIA500); anterior chamber depth (ACD); iris-lens contact distance (ILCD), and iris configuration were analyzed with the built-in software and a customized program.

Results. The ACA parameters were not significantly different among all three groups in the dark. The PEX eyes had significantly smaller ACA parameters than their fellow eyes and normal control eyes in the light. PEX eyes also had significantly shallower ACD, longer ILCD, and greater iris convexity (both in dark and light), and thinner iris (in dark) than their fellow eyes. The fellow eyes had significantly lower ACD both in the dark and light, and smaller angle opening distance at 500 μm and ILCD in the light than normal controls. There were no significant differences in the iris area among the three groups.

Conclusions. Differences in the anterior segmental morphology are present between PEX and fellow eyes. These disparities may be related to the asymmetry in patients with the unilateral PEX syndrome. (*Invest Ophthalmol Vis Sci.* 2011;52:5679-5684) DOI:10.1167/iovs.11-7274

The pseudoexfoliation (PEX) syndrome is a common age-related disorder of the extracellular matrix that can affect 10%-20% of people older than 60 years worldwide.[1,2] The main ocular manifestation of PEX is the production and progressive accumulation of abnormal extracellular fibrillar and pseudoexfoliation material in almost all of the inner walls of the anterior segment of the eye. There has been a renewed interest in this disease because of the better awareness of the complications accompanying PEX including phacodonesis and lens subluxation, intractable glaucoma, melanin dispersions, poor mydriasis, blood-aqueous barrier dysfunction, and posterior synechiae.[1,2]

Up to 76% of patients with PEX are initially diagnosed as having unilateral PEX.[3] However in an electron microscopic study, Parekh et al. reported that 26 of 32 patients (81%) with clinically unilateral PEX had pseudoexfoliation material on either the lens capsule or conjunctival samples of the clinically unaffected eyes.[4] Furthermore, several reports on the follow-up of patients with unilateral PEX documented that 74% to 81.6% of the unilateral cases became bilateral.[5-7] This suggested that unilateral PEX is in fact a bilateral but asymmetric condition, and the percentage of unilateral disease decreases with a corresponding increase in bilateral disease with increasing age. The factors affecting the conversion from unilateral to bilateral disease are not known, and the pathogenic mechanism underlying the asymmetric condition has not been determined. Subtle differences in ocular blood flow,[8] aqueous humor dynamics, blood-aqueous barrier function, or anterior segmental morphology might be responsible for the asymmetry.[1,2]

Ultrasound biomicroscopic (UBM) studies on the morphologic alterations of the anterior segment of PEX eyes have shown abnormalities of the zonules, lens thickening, shallow central anterior chamber depth (ACD), and occludable angles.[9-14] In unilateral PEX patients, the PEX eyes and fellow eyes have been reported to share some similar morphologic changes.[14]

With the advancement of ophthalmic imaging instruments, more information has been obtained on the morphology of the structures in different ocular disorders. Fourier domain anterior segment optical coherence tomography (AS-OCT) is a representative imaging technique that provides cross-sectional views of the anterior segment with a resolution better than that of UBM.[15] Images and measurements of very fine structures can be achieved rapidly and noninvasively. In addition, using the AS-OCT video mode has allowed investigators to document dynamic morphologic alterations of the anterior chamber angle (ACA) and iris during pupillary movements without being influenced by accommodation.[16-18]

The purpose of this study was to compare the morphology of the anterior segment of affected eyes and their fellow eyes in cases of unilateral PEX. To accomplish this, we recorded images of the anterior segment by AS-OCT during pupillary dilation and constriction. Comparisons were made of the ACA

From the [1]Department of Ophthalmology, Ehime University School of Medicine, Toon City, Ehime, Japan; [2]Department of Ophthalmology, University of the Ryukyus Hospital, Okinawa, Japan; and [3]Department of Ophthalmology, Takanoko Hospital, Matsuyama, Ehime, Japan.

Submitted for publication January 25, 2011; revised March 16, 2011; accepted April 19, 2011.

Disclosure: **X. Zheng**, None; **H. Sakai**, None; **T. Goto**, None; **K. Namiguchi**, None; **S. Mizoue**, None; **A. Shiraishi**, None; **S. Sawaguchi**, None; **Y. Ohashi**, None

Corresponding author: Xiaodong Zheng, Department of Ophthalmology, Ehime University School of Medicine, Ehime 791-0295, Japan; xzheng@m.ehime-u.ac.jp.

and the iris parameters in the PEX eyes, their fellow eyes, and normal control eyes.

Subjects and Methods

Patients and Control Subjects

We studied 45 consecutive patients with unilateral PEX syndrome who visited the Department of Ophthalmology, Ehime University from January 2009 to November 2010. All eyes were examined by slit-lamp biomicroscopy after pupillary dilation. PEX eyes had clinically evident PEX material at the pupillary border or on the anterior lens capsule in one eye. These eyes were placed in the PEX eye group. Their clinically unaffected fellow eyes were placed in the fellow eye group. Forty-five age- and sex-matched normal subjects were also studied and one eye was randomly selected as the normal control.

The exclusion criteria included: prior intraocular surgery, e.g., laser trabeculoplasty, laser iridotomy, laser iridoplasty, or ocular trauma; evidence of peripheral anterior synechiae on indentation; iris dystrophy or dyscoria; lymphoma, sarcoidosis, diabetic mellitus, inflammation; eyes using anti-glaucoma medications or having abnormal intraocular pressure; or use of systemic medications that could affect the ACA or pupillary reflex.

All participants underwent a complete ophthalmic examination, including best-corrected visual acuity, autorefraction, slit-lamp microscopy, and intraocular pressure measurements by applanation tonometry (Goldmann; Haag-Streit, Köniz, Switzerland). The ocular axial length was measured (IOL Master; Carl Zeiss, Jena, Germany). Gonioscopy was performed with a 4-mirror lens at high magnification (×16) with the eye in the primary position of gaze. All investigated eyes had open-angles and all structures anterior to the scleral spur were identified by gonioscopy (Shaffer grade ≧ 2).

The procedures used conformed to the tenets of the Declaration of Helsinki. An informed consent was obtained from all subjects after an explanation of the nature and possible consequences of the procedures. The protocol used was approved by the Ethics Committee of Ehime University School of Medicine.

Anterior Segment Optical Coherence Tomography

An experienced operator who was masked to the results of the ophthalmic examinations performed the AS-OCT (Swept-source 1000 CASIA AS-OCT, Tomey, Nagoya, Japan). This AS-OCT system had a 30 kHz axial scan rate with an axial resolution of 10 μm. The use of 1310 nm wavelength coupled with high resolution Fourier domain-OCT improved the resolution and penetration of the measuring beam into turbid tissues with a scan depth of 6 mm. This was sufficient to image the entire anterior segment in one frame.[15] The scan of the anterior chamber was a noncontact procedure during which the subject fixated on an internal target.

The AS-OCT real-time video recording mode (4 frames per second) was used to study the changes of the ACA and the iris during pupillary dilation and light-induced constriction. The scan was centered on the pupil, and the scan passed along the nasal-temporal axis, i.e., 0° to 180°. After one minute at 50 lux of dark-adaptation, a LED pen light (Gentos, Tokyo, Japan), fixed at a distance of 20 cm, 45° from the optic axis of the examined eye, was turned on. The illuminance of the light was standardized at 2000 lux, and it was kept on for 4 seconds to induce pupillary constriction. AS-OCT scans were recorded for 10 seconds and the operator chose the best video frame with good centering to analyze. Data were excluded if the scleral spur could not be identified or the frame was of suboptimal quality because of blinks and eye movements. Each eye was examined three times with an intertest interval of at least 10 minutes.

Image Processing

All images were processed separately and analyzed by two observers (XZ and KN) who were masked to the clinical findings of the eye. The video file was reviewed and one frame of the images in the dark (most dilated pupil) and the light (most constricted pupil) were selected for each subject. The morphology of structures on the nasal side of the eye was analyzed. Images were first analyzed with the built-in software for the ACA parameters: angle opening distance at 500 μm (AOD500), trabecular-iris space at 500 μm (TISA500), and trabecular-iris angle at 500 μm (TIA500). The central anterior chamber depth (ACD) and the pupillary diameter were also measured (Fig. 1A).

All images were then exported and analyzed with a customized software program written for the following iris parameters (Fig. 1B): the iris thickness in the dilator muscle region (DMR) which was set at one-half of the distance between the scleral spur and the pupillary margin was measured as described[19]; and the iris thickness in the sphincter muscle region (SMR) which was set at 0.75 mm from the pupillary margin was also measured. The ratio of the thickness at

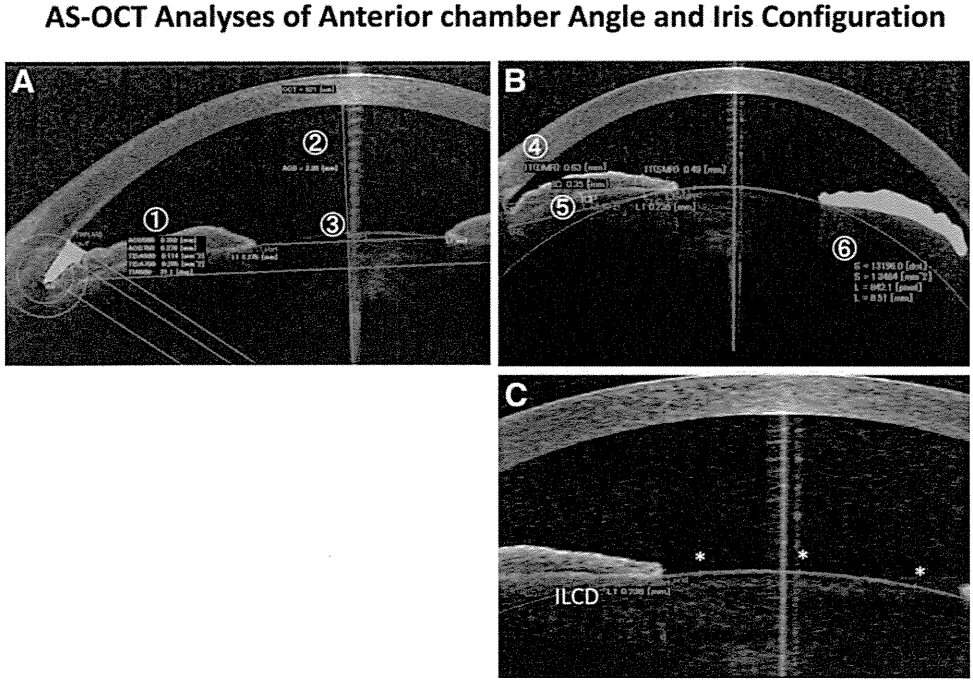

FIGURE 1. Anterior segment optical coherence tomographic (AS-OCT) images from which the morphologic parameters of the structures in the anterior chamber and the iris were measured. (**A**) Anterior chamber parameters of (1) angle measurements (AOD500, TISA500, and TIA500 were used), (2) central anterior chamber depth (ACD), and (3) pupillary diameter. (**B**) Iris configurations of (4) iris thickness (IT) at the dilator muscle region (DMR) measured at one-half of the distance between the scleral spur (SS) and the pupillary margin; iris thickness at the sphincter muscle region (SMR) measured at 0.75 mm from the pupillary margin, (5) iris convexity (IC), and (6) iris area (indicated by *green shading* over the right half of the iris). (**C**) Iris-lens contact distance (ILCD) measurement. *Asterisks* represent three points selected on the lens surface for generating estimated curved line of the anterior lens capsule. The ILCD was measured along the iris pigment epithelium from the papillary border to the point at which the iris was seen to separate from the anterior lens capsule.

the DMR and SMR (DMR/SMR) was used for the statistical analyses to reduce the intersubject variability.

In addition, the iris convexity was defined as the distance between the posterior point of greatest iris curvature to a line drawn from the most peripheral to the most central points of the iris pigment epithelium. The area of the iris was determined by the cumulative cross-sectional area of the iris from the scleral spur to the edge of the pupil.[20] A program was also written for the calculation of iris-lens contact distance (ILCD). To measure this, 3 points were manually designated on the lens surface and a curved line of the anterior lens capsule was automatically generated by the software. The ILCD was measured along the iris pigment epithelium from the pupillary border to the point at which the iris was seen to separate from the anterior lens capsule (Fig. 1C). These measurements had good reliability with the intraobserver and interobserver intraclass correlation coefficients ranging between 0.96 to 0.98 and 0.97 to 0.99, respectively.

Statistical Analyses

All data are expressed as the means ± standard deviations (SDs). Gender differences between PEX patients and normal subjects were evaluated by the χ^2 test. Comparisons of other demographic data, biometric characteristics, and AS-OCT parameters were evaluated by paired *t*-tests (PEX eye versus fellow eye) or two-tailed Student's *t*-tests (PEX eye versus normal control eye or fellow eye versus normal control eye). The ACA and iris parameters were compared with adjustment for pupil size. The significance of the differences in the DMR/SMR ratio among the three groups was determined by the Tukey-Kramer test. A probability level of $P < 0.05$ was considered statistically significant. Data were analyzed with statistical software (JMP version 9.0 for Windows; SAS Japan Inc., Tokyo, Japan).

Results

Three patients with unilateral PEX and three normal subjects were excluded due to a poor imaging of the scleral spur. Forty-two patients (17 men and 25 women with a mean age of 72.7 ± 7.4 years and a range of 61 to 92 years) and 42 normal subjects (16 men and 26 women with a mean age of 73.6 ± 8.9 years and a range of 64 to 90 years) were analyzed. The mean age of the PEX patients was not significantly different from that of the normal controls ($P = 0.886$, two-tailed Student's *t*-test). Slit-lamp biomicroscopy showed that all eyes with PEX had typical whitish exfoliation material at the pupillary edge and on the anterior lens capsule. The fellow eyes and normal control eyes did not have these deposits. The differences in the visual acuity, gender distribution, refractive error (spherical equivalent), axial length, intraocular pressure, and gonioscopic grading (Shaffer) of the ACA among the three groups were not significant. The data are summarized in Table 1.

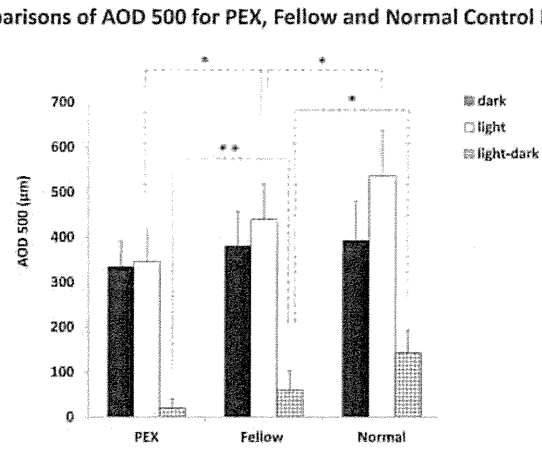

Figure 2. Comparisons of AOD500 for eyes with the PEX syndrome, their unaffected fellow eyes, and normal control eyes. Dark, values measured in the dark when pupils were mostly dilated; Light, values measured in the light when pupils were mostly constricted; Light-dark, $AOD500_{(light)} - AOD500_{(dark)}$. Statistical significance is denoted by $^{**}P < 0.01$, and $^{*}P < 0.05$.

Anterior Chamber Angle (ACA) Morphology

In the dark when pupils were dilated, the mean AOD500 was 333.6 ± 56.5 μm in the PEX eyes, 380.1 ± 76.4 μm in the fellow eyes, and 392.6 ± 87.2 μm in the normal control eyes (Fig. 2). The differences between the three groups were not significant (PEX versus fellow, $P = 0.225$, paired *t*-tests; PEX versus normal, $P = 0.133$; and fellow versus normal, $P = 0.416$, both two-tailed Student's *t*-test). When the pupils were constricted by light, the AOD500 in the PEX eyes was significantly smaller than that of the fellow eyes ($P = 0.021$) and the normal eyes ($P = 0.008$). The AOD500 in the fellow eyes was also significantly smaller than that of the normal eyes ($P = 0.037$). In addition, the mean dark-to-light change of the AOD500 for the PEX eyes was also significantly less than that of the fellow eyes (20.5 ± 16.6 μm vs. 60.8 ± 42.2 μm; $P = 0.007$) and of the normal control eyes ($P = 0.004$). The difference in the changes of the AOD500 between the fellow and normal control eyes was also significant ($P = 0.033$).

In the dark, the TISA500 was not significantly different among the three groups. However in light, the TISA500 of the PEX eyes was significantly smaller than that of the fellow eyes and normal control eyes (Fig. 3).In the light, the PEX eyes also had significantly narrower TIA500 than that of the fellow and normal control eyes. Similarly, the dark-to-light change of the TIA500 of the PEX eyes was significantly less than that of the

Table 1. Demographic and Biometric Characteristics of PEX Eye, Fellow Eye, and Normal Control Eye Groups

	PEX	Fellow	Normal	*P*
Age, y	72.7 ± 7.4	—	73.6 ± 8.9	0.886*
Sex, male/female	17/25	—	16/26	0.763†
Spherical equivalent, D	−0.34 ± 2.8	−0.22 ± 1.76	−0.28 ± 1.52	0.521‡
BCVA, LogMAR	0.04 ± 0.05	0.03 ± 0.04	0.00 ± 0.03	0.554‡
Axial length, mm	23.71 ± 0.94	24.06 ± 0.81	24.5 ± 1.01	0.669‡
Intraocular pressure, mm Hg	14.8 ± 3.1	13.6 ± 3.8	13.1 ± 4.8	0.375‡
Gonioscopy grading (Shaffer)	2.9 ± 0.68	3.1 ± 0.77	3.1 ± 0.82	0.428‡

Data are given as mean ± SD. All groups, $n = 42$. BCVA, best-corrected visual acuity; D, Diopter; LogMAR, logarithm of the minimum angle of resolution.

* PEX patients versus normal control subjects (two-tailed Student's *t*-test).

† PEX patients versus normal control subjects (χ^2).

‡ PEX eye versus fellow eye (paired *t*-test).

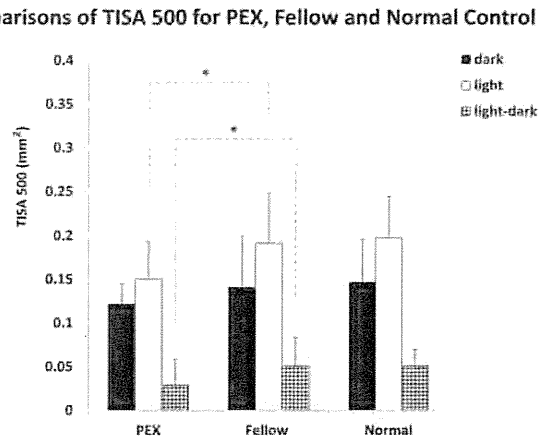

FIGURE 3. Comparisons of TISA500 for eyes with the PEX syndrome, their unaffected fellow eyes, and normal control eyes. Dark, values measured in the dark when pupils were mostly dilated; Light, values measured in the light when pupils were mostly constricted; Light-dark, $TISA500_{(light)} - TISA\ 500_{(dark)}$. Statistical significance is denoted by $^{*}P < 0.05$.

fellow eyes (Fig. 4). The PEX eyes had significantly smaller ACD than that of the fellow eyes both in dark and light ($P = 0.021$ and $P = 0.018$, respectively; paired *t*-tests; Table 2). The ACD of the fellow eyes was also significantly smaller than that of normal control eyes ($P = 0.038$ and $P = 0.032$ for dark and light respectively; two-tailed Student's *t*-test).

The pupillary diameter in dark for the PEX eyes was significantly smaller than that of fellow eyes ($P = 0.011$). When the dark-to-light change was analyzed, the PEX eyes had significantly less pupillary change than that of the fellow eyes ($P = 0.025$) and the normal control eyes ($P = 0.008$).

Iris Configuration

The difference in the area of the iris was not significant among the three groups either in dark or light. The mean iris convexity of the PEX eyes was 286.3 ± 63.7 μm in the dark and 251.5 ± 72.4 μm in the light. The mean iris convexity of the fellow eyes was 239.4 ± 86.6 μm in the dark and 195.1 ± 59.3 μm in the light. The iris convexity was significantly greater in the PEX eyes than that of their fellow eyes both in the dark and the light ($P = 0.029$ and $P = 0.038$, respectively; paired *t*-tests). The convexity of the iris of the fellow eyes was also larger than that of the normal controls but the difference was not significant.

The DMR/SMR ratio in dark for PEX eyes was significantly less than that of the fellow eyes ($P = 0.037$; Tukey-Kramer test). The differences in the DMR/SMR ratio among the three groups in light were not significant (Table 2).

Iris-Lens Contact Distance (ILCD)

The mean ILCD of PEX eyes was 0.523 ± 0.14 mm in the dark and 0.908 ± 0.15 mm in the light. The mean ILCD of the fellow eyes was 0.346 ± 0.12 mm in the dark and 0.732 ± 0.11 mm in the light. The differences in the ILCD between PEX and fellow eyes were significant both in dark and light ($P < 0.001$ for both; paired *t*-tests; Figure 5). In the light, the ILCD of the fellow eyes was also significantly longer than that of normal control eyes ($P = 0.035$; two-tailed Student's *t*-tests; Fig. 5).

Discussion

Our findings showed that AS-OCT can be used for noninvasive, quantitative, and reliable analyses of the ACA and iris morphology in eyes with the PEX syndrome. These findings would probably not be obtained by regular gonioscopy or slit-lamp examination. Analyzing the video files provided us with a useful method to accurately examine the ACA and iris configuration when the pupil was most dilated or constricted. This then allowed us to detect subtle changes between the dark and light conditions.

The differences in the ACA parameters, namely, the AOD500, TISA500, and TIA500, among the three groups were not significant in the dark. However, when the pupil was constricted by light, the PEX eyes had significantly smaller values for all the ACA parameters indicating that the widening of the ACA was significantly more impaired in PEX eyes than in their fellow eyes or normal controls. These findings combined with the smaller ACD in PEX eyes indicate the possibility of a weakness of the zonular fibers and forward shifting of the lens, which is consistent with the previous UBM studies.[10–14] For our PEX patients, although the lens shifting was too small to cause a statistically significant change in the refraction, this alteration could be detected by the highly sensitive AS-OCT analysis.

It is known that melanin granules derived from the iris pigment epithelium and PEX deposits form posterior synechiae starting from the early stages of the PEX process.[1,2] These morphologic changes may account for the poor mydriasis, increased iridolenticular contact, and decreased ability of ACA widening during pupillary constriction.

On the other hand, these morphologic alterations may be pathogenic factors for PEX development or the cause for PEX progression in the PEX process. The morphologic changes may also lead to decreased blood flow or circulatory disturbances resulting in abnormalities in the microenvironment of the anterior chamber such as hypoxia and elevation of cellular stress.[1,2,8] Increased pathologic cytokine or chemokine levels, hypoxic conditions, and circulatory factors in the anterior segment of the eye may also play pivotal roles in the progression of PEX. The relationships among these factors with the morphologic changes need to be investigated.

The iris-lens contact distance (ILCD) was also compared among the three groups. Although ultrasound microscopy can be used for direct measurements of ILCD,[21–23] our study provided a rapid, noncontact method in evaluating this parameter by AS-OCT imaging. The use of Fourier domain AS-OCT provided excellent images of the iris configuration and in combi-

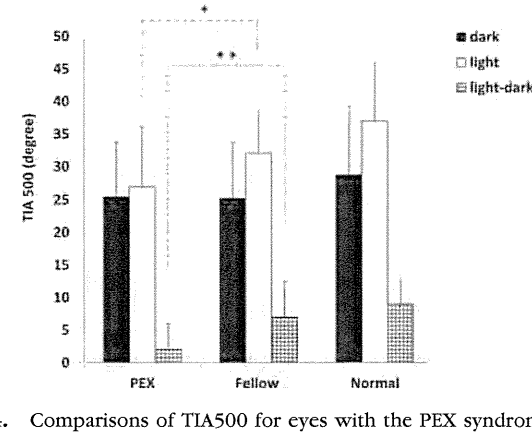

IGURE 4. Comparisons of TIA500 for eyes with the PEX syndrome, their unaffected fellow eyes, and normal control eyes. Dark, values measured in the dark when pupils were mostly dilated; Light, values measured in the light when pupils were mostly constricted; Light-dark, $TIA500_{(light)} - TIA500_{(dark)}$. Statistical significance is denoted by $^{**}P < 0.01$, and $^{*}P < 0.05$.

TABLE 2. Comparisons of Anterior Chamber Depth and Iris Configuration Parameters for PEX, Fellow, and Normal Control Eyes

	PEX	Fellow	Normal	*P*
ACD				
Dark, mm	2.52 ± 0.36	2.71 ± 0.34*	2.89 ± 0.36	0.021†
Light, mm	2.52 ± 0.29	2.72 ± 0.23*	2.89 ± 0.48	0.018†
Pupillary diameter				
Dark, mm	3.61 ± 0.46	5.08 ± 0.41	5.86 ± 0.71	0.011†
Light, mm	2.73 ± 0.53	2.68 ± 0.55	2.61 ± 0.52	0.489†
Pupil change (Dark-Light, mm)	1.04 ± 0.48	1.57 ± 0.62	1.55 ± 0.51	0.025†
Iris area				
Dark, mm^2	1.371 ± 0.27	1.368 ± 0.26	1.473 ± 0.24	0.117†
Light, mm^2	1.635 ± 0.36	1.589 ± 0.31	1.688 ± 0.21	0.276†
Iris Convexity				
Dark, μm	286.3 ± 63.7	239.4 ± 86.6	212.7 ± 81.4	0.029†
Light, μm	251.5 ± 72.4	195.1 ± 59.3	180.3 ± 87.3	0.038†
DMR/SMR Ratio				
Dark	0.81 ± 0.12	0.92 ± 0.17	0.97 ± 0.21	0.037‡
Light	0.86 ± 0.21	0.88 ± 0.14	0.87 ± 0.13	0.133‡

Data are given as mean ± SD. Each group, $n = 42$. ACD and iris area analyses were adjusted by pupil size.

* Significantly different compared with normal control eye ($P < 0.05$; two-tailed Student's *t*-test).

† PEX eye versus fellow eye (paired *t*-test).

‡ PEX eye versus fellow eye (Tukey-Kramer test).

nation with our customized software, we were able to measure the ILCD reliably with high intra- and interobserver intraclass correlation coefficients.

Our findings showed that the ILCD was significantly longer in the PEX eyes than that of their fellow eyes both when the pupil was dilated and when it was constricted. The difference was also found when fellow eyes were compared with normal control eyes with the pupil constricted. The fact that PEX material is often observed at the pupillary border and on the lens capsular area of pupillary movements suggest the production of visible PEX material may be associated with iridolenticular friction. In a separate study, our data showed that PEX eyes with longer intermediate zone, the area between central disc of PEX material on the lens capsule and peripheral granular zone, tended to have longer ILCD ($r = 0.584$, Spearman's correlation coefficient; $P = 0.006$) and higher iris convexity ($r = 0.649$; $P = 0.002$). The relationship between the morphologic alterations of the iris and the progression of PEX syndrome remains to be investigated. We suggest that the increased iris-lens contact and iris convexity may be related to increased iridolenticular friction and increased PEX material formation leading to inflammatory responses. As a result, PEX-related cytokines or chemokines can be released to trigger or further accelerate the process.[24-26]

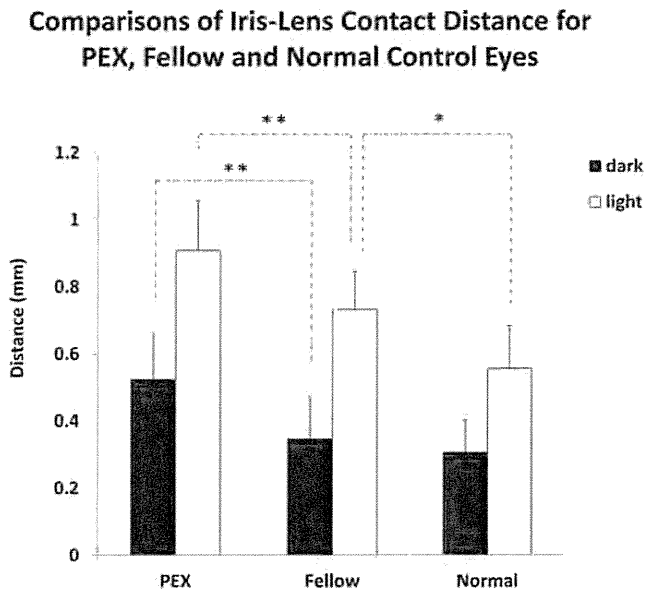

FIGURE 5. Comparisons of iris-lens contact distance for eyes with the PEX syndrome, their unaffected fellow eyes, and normal control eyes. Dark, values measured in the dark when pupils were mostly dilated; Light, values measured in the light when pupils were mostly constricted. Statistical significance is denoted by $^{**}P < 0.01$, and $^{*}P < 0.05$.

The clinical significance of our results are: first, the AS-OCT parameters, e.g., increased ILCD and decreased widening of the angle during pupillary movements, may be used as additional evidence for an early diagnosis of PEX. In addition, identifying these patients before surgery can help the cataract surgeon be prepared for potential problems, and glaucoma specialist to better manage the ocular pressure and reduce the progression of eyes that would ordinarily be diagnosed as normal, ocular hypertensive, or having primary open angle glaucoma.[27] Second, our AS-OCT analysis indicates that it is a rapid, noninvasive, and quantitative method for following and evaluating the severity of the PEX process. It would be interesting to conduct a prospective study on PEX suspects with AS-OCT to follow the conversion from unilateral PEX to bilateral disease. Third, if the morphologic alterations are the pathogenic factors for PEX development or progression, cataract extraction to reduce the ILCD and to widen the angle might be considered to prevent the progression of ocular PEX. Evidence is accumulating to show the effects of cataract surgery on a reduction of intraocular pressure and possibly reducing the number of patients with PEX glaucoma who progress to medication or surgery.[28,29] Future studies are needed for long-term follow-up on PEX patients to observe the PEX progression after cataract surgery.

There are some limitations of this study. First, this was a comparative correlation study, and a causal relationship between alterations of the morphologic parameters and the PEX development was not determined. The argument certainly remains that the morphologic alterations observed in this study could be the result of the asymmetric manifestation. Thus, a

study designed to test the null hypothesis that the morphologic parameters of the structures in the anterior chamber do not cause or promote PEX must be tested before the "chicken-or-egg" question can be solved. However, our findings showed that the fellow eyes also had the same tendency of morphologic alterations. Therefore, it is reasonable to suggest that the morphologic alterations might take place earlier at least before the clinically evident PEX manifestation.

Second, although the morphologic changes observed might be caused by PEX, they might be the clinical features of the shallow ACD with poor pupillary dilation. In our study, comparing with PEX eyes and their fellow eyes, because PEX is the most discernible difference that can be appreciated by slit-lamp microscopy, it is possible to correlate the morphologic changes to be PEX-related.

Third, our study is limited because it is a cross-sectional study, and was performed on the morphology of structures on the nasal side of the eye. Because this affected all groups equally, our study also showed similar results in other radial directions, and changes in nasal direction are known to take place earlier in the PEX process.[30] Therefore, we believe that this limitation has a small effect on our results.

In summary, our study showed that PEX eyes had narrower anterior chamber angle, decreased angle widening during pupillary movements, and increased iridolenticular contact and iris convexity. The fellow eyes shared similar features to some degree. PEX is bilaterally involved; the morphologic differences in the anterior segmental anatomy between the two eyes may be related to the asymmetric manifestation in clinically unilateral PEX.

References

1. Naumann GOH, Schlötzer-Schrehardt U, Küchle M. Pseudoexfoliation syndrome for the comprehensive ophthalmologist: Intraocular and systemic manifestations. *Ophthalmology.* 1998;105:951-968.
2. Schlötzer-Schrehardt U, Naumann GOH. Ocular and systemic pseudoexfoliation syndrome. *Am J Ophthalmol.* 2006;141:921-937.
3. Kozart DM, Yanoff M. Intraocular pressure status in 100 consecutive patients with exfoliation syndrome. *Ophthalmology.* 1982;89:214-218.
4. Parekh P, Green WR, StarK WJ, Akpek EK. Electron microscopic investigation of the lens capsule and conjunctival tissues in individuals with clinically unilateral pseudoexfoliation syndrome. *Ophthalmology.* 2008;115:614-619.
5. Slagsvold JE. The follow-up in patients with pseudoexfoliation of the lens capsule with and without glaucoma. 2. The development of glaucoma in persons with pseudoexfoliation. *Acta Ophthalmol (Copenh).* 1986;64:241-245.
6. Aasved H. Mass screening for fibrillopathia epitheliocapsularis, so-called senile exfoliation or pseudoexfoliation of the anterior lens capsule. *Acta Ophthalmol (Copenh).* 1971;49:334-343.
7. Kozobolis VP, Papatzanaki M, Vlachonikolis IG, et al. Epidemiology of pseudoexfoliation in the island of Crete (Greece). *Acta Ophthalmol Scand.* 1997;75:726-729.
8. Dayanir V, Topaloglu A, Ozsunar Y, et al. Orbital blood flow parameters in unilateral pseudoexfoliation syndrome. *Int Ophthalmol.* 2009;29:27-32.
9. Pavlin CJ, Harasiewicz K, Sherar MD, et al. Clinical use of ultrasound biomicroscopy. *Ophthalmology.* 1991;98:287-295.
10. Damji KF, Chialant D, Shah K, et al. Biometric characteristics of eyes with exfoliation syndrome and occludable as well as open angles and eyes with primary open-angle glaucoma. *Can J Ophthalmol.* 2009;44:70-75.
11. Ritch R, Vessani RM, Tran HV, et al. Ultrasound biomicroscopic assessment of zonular appearance in exfoliation syndrome. *Acta Ophthalmol Scand.* 2007;85:495-499.
12. Guo S, Gewirtz M, Thaker R, Reed M. Characterizing pseudoexfoliation syndrome through the use of ultrasound biomicroscopy. *J Cataract Refract Surg.* 2006;32:614-617.
13. Inazumi K, Takahashi D, Taniguchi T, Yamamoto T. Ultrasound biomicroscopic classification of zonules in exfoliation syndrome. *Jpn J Ophthalmol.* 2002;46:502-509.
14. Sbeity Z, Dorairaj SK, Reddy S, et al. Ultrasound biomicroscopy of zonular anatomy in clinically unilateral exfoliation syndrome. *Acta Ophthalmol.* 2008;86:565-568.
15. Steinert R, Huang D. *Anterior Segment Optical Coherence Tomography.* 1st ed. Thorofare, NJ: Slack; 2008.
16. Leung CKS, Cheung CYL, Li LC, et al. Dynamic analysis of dark-light changes of the anterior chamber angle with anterior segment OCT. *Invest Ophthalmol Vis Sci.* 2007;48:4116-4122.
17. Quigley HA, Silver DM, Friedman DS, et al. Iris cross-sectional area decreases with pupil dilation and its dynamic behavior is a risk factor in angle closure. *J Glaucoma.* 2009;18:173-179.
18. Cheung CY, Liu S, Weinreb RN, et al. Dynamic analysis of iris configuration with anterior segment optical coherence tomography. *Invest Ophthalmol Vis Sci.* 2010;51:4040-4046.
19. Prata TS, Palmiero PM, Angelilli AA, et al. Iris morphologic changes related to α1-adrenergic receptor antagonists. Implications for intraoperative floppy iris syndrome. *Ophthalmology.* 2009;116:877-881.
20. Wang B, Sakata LM, Friedman DS, et al. Quantitative iris parameters and association with narrow angles. *Ophthalmology.* 2010;117:11-17.
21. Breingan PJ, Esaki K, Ishikawa H, et al. Iridolenticular contact decreases following laser iridotomy for pigment dispersion syndrome. *Arch Ophthalmol.* 1999;117:325-328.
22. Foster FS, Pavlin CJ, Harasiewicz KA, et al. Advances in ultrasound biomicroscopy. *Ultrasound Med Biol.* 2000;26:1-27.
23. Pavlin CJ. Practical application of ultrasound biomicroscopy. *Can J Ophthalmol.* 1995;30:225-229.
24. Zenkel M, Lewczuk P, Jünemann A, et al. Proinflammatory cytokines are involved in the initiation of the abnormal matrix process in pseudoexfoliation syndrome/glaucoma. *Am J Pathol.* 2010;176:2868-2879.
25. Schlötzer-Schrehardt U, Zenkel M, Kuchle M, Sakai LY, Naumann GOH. Role of transforming growth factor-β1 and its latent form binding protein in pseudoexfoliation syndrome. *Exp Eye Res.* 2001;73:765-780.
26. Koliakos GG, Konstas AGP, Schlötzer-Schrehardt U, et al. Endothelin-1 concentration is increased in the aqueous humour of patients with exfoliation syndrome. *Br J Ophthalmol.* 2004;88:523-527.
27. Prince AM, Streeten BW, Ritch R, Dark AJ, Sperling M. Preclinical diagnosis of pseudoexfoliation syndrome. *Arch Ophthalmol.* 1987;105:1076-1082.
28. Shingleton BJ, Laul A, Nagao K, et al. Effect of phacoemulsification on intraocular pressure in eyes with pseudoexfoliation: Single-surgeon series. *J Cataract Refract Surg.* 2008;34:1834-1841.
29. Mamalis N. Exfoliation syndrome: effects of cataract surgery on glaucoma. *J Cataract Refract Surg.* 2008;34:1813-1814.
30. Tetsumoto K, Schlötzer-Schrehardt U, Küchle M, et al. Precapsular layer of the anterior lens capsule in early pseudoexfoliation syndrome. *Graefes Arch Clin Exp Ophthamol.* 1992;230:252-257.

Mathematical Projection Model of Visual Loss Due to Fuchs Corneal Dystrophy

Shin Hatou,[1] Shigeto Shimmura,[1] Jun Shimazaki,[2] Tomohiko Usui,[3] Shiro Amano,[3] Hideaki Yokogawa,[4] Akira Kobayashi,[4] Xiaodong Zheng,[5] Atsushi Shiraishi,[5] Yuichi Ohashi,[5] Tsutomu Inatomi,[6] and Kazuo Tsubota[1]

Purpose. To devise a mathematical disease classification model for eyes with primary guttata cornea, on the bases of endothelial loss trajectory and probability of advanced disease.

Methods. A series of 1971 patients (3281 eyes), some with and some without guttata corneas, undergoing specular microscopy were retrospectively reviewed. The eyes were classified into four stages; stage 0, without guttae; 1, guttata cornea without edema; 2, mild Fuchs' corneal dystrophy (FCD); and 3, severe FCD, according to clinical records, and patient age and corneal endothelial cell density (ECD) were plotted. Nonparametric density smoothing was used to create a contour map, and a best-fit curve for ECD loss was calculated. The relation between ECD decrease rate and the stages were evaluated.

Results. Endothelial decrease rate in stage 0 was 0.44%/year, which was compatible with that of normal eyes reported in previous studies. Decrease rates of stages 1, 2, and 3 were 0.81%, 2.65%, and 3.08%/ year, respectively. The age-ECD loss curves of 1.40%/year ($ECO_{1.4}$) and 2.00%/year ($ECO_{2.0}$) further divided stage 1 into three subgroups; stage 1a, asymptomatic guttata cornea; 1b, borderline guttata cornea; and 1c, pre-FCD. The $ECO_{2.0}$ cutoff line differentiated eyes with FCD from those without edema with a sensitivity and specificity of >90%. Stage 1c eyes were below $ECO_{2.0}$ and had a decrease rate as high as FCD.

Conclusions. This mathematical model can be used to predict the prognosis of patients with primary guttata cornea. (*Invest Ophthalmol Vis Sci.* 2011;52:7888-7893) DOI:10.1167/iovs.11-8040

From the [1]Department of Ophthalmology, Keio University School of Medicine, Shinjuku, Japan; the [2]Department of Ophthalmology, Tokyo Dental College Ichikawa General Hospital, Tokyo, Japan; the [3]Department of Ophthalmology, Tokyo University School of Medicine, Tokyo, Japan; the [4]Department of Ophthalmology, Kanazawa University School of Medicine, Kanazawa, Japan. the [5]Department of Ophthalmology, Ehime University School of Medicine, Matsuyama, Japan; and the [6]Department of Ophthalmology, Kyoto Prefectural University of Medicine, Kyoto, Japan.

Supported by a grant from the Ministry of Health, Labor and Welfare, Japan. The sponsor or funding organization had no role in the design or conduct of this research.

Submitted for publication June 14, 2011; revised August 8, 2011; accepted August 12, 2011.

Disclosure: **S. Hatou**, None; **S. Shimmura**, None; **J. Shimazaki**, None; **T. Usui**, None; **S. Amano**, None; **H. Yokogawa**, None; **A. Kobayashi**, None; **X. Zheng**, None; **A. Shiraishi**, None; **Y. Ohashi**, None; **T. Inatomi**, None; **K. Tsubota**, None

Corresponding author: Shigeto Shimmura, Department of Ophthalmology, Keio University School of Medicine, 35 Shinanomachi, Shinjuku, Tokyo 160-8582, Japan;shige@sc.itc.keio.ac.jp.

Fuchs' corneal dystrophy (FCD) is a progressive, bilateral corneal dystrophy.[1] There is a progressive loss of corneal endothelial cells with secretion of an abnormally thickened basement membrane, leading to corneal guttae formation.[1] On specular microscopy, these corneal guttae are observed as dark areas.[1,2] As endothelial function deteriorates, corneal edema increases and visual acuity declines,[2] and FCD is a major indication for keratoplasty (corneal transplants) in the United States.[3-5] Although FCD is recognized as a dominantly inherited disorder, females are predisposed to it and develop corneal guttae 2.5 times more frequently than do males, progressing to corneal edema 5.7 times more often than do males.[6] The prevalence of primary guttata cornea and FCD are lower in Japan than in the United States.[7,8] This difference in prevalence is thought to be mainly attributable to the racial difference.[7]

Primary guttata cornea is believed to be a preliminary stage of FCD. Krachmer et al.[6] graded guttata cornea and FCD according to a spread of guttae and reported that there was a positive correlation between age and grade of guttae. However, the exact natural course of guttata cornea, or whether all cases of guttata cornea progress to FCD remains to be determined. A prospective study that follows the decline in endothelial cells density (ECD) with age would be ideal for predicting the natural course of guttata cornea; however, a very long follow-up would be required, and recruiting asymptomatic potential patients is practically impossible, especially in Japan. A retrospective study with a large database and an adequate mathematical model can be used in a similar way to predict the prognosis of patients with guttata cornea. In this report, we retrospectively reviewed age and ECD in a large group of hospital-based patients and evaluated the prevalence of guttae, male:female ratio, and distribution of age and ECD. In addition, we propose a new classification of guttata cornea based on a mathematical model that adequately predicts the prognosis of disease.

Methods

Subjects

Clinical records of outpatients who underwent specular microscopy for corneal endothelial cell counts from January through December 2009 in six hospitals affiliated with the Fuchs' Corneal Dystrophy Study Group of Japan were retrospectively reviewed. The purpose of specular microscopy for those patients were routine examination before ocular surgery, follow-up for corneal diseases that were thought to have little effect on endothelium (such as keratoconus or lattice corneal dystrophy), or follow-up for diagnosed Fuchs' corneal dystrophy. Patients who had a history of trauma, corneal infection, intraocular inflammation, intraocular surgery, or laser iridotomy were excluded from the study. Endothelial photographs were taken at the center of the pupillary area with a noncontact specular microscope (Nonkon Robo F & A; Konan Medical, Nishinomiya, Japan, or EM-3000; Tomey,

Investigative Ophthalmology & Visual Science, October 2011, Vol. 52, No. 11

Nagoya, Japan), and analyses of the photographs were performed with an automatic cell analysis system attached to the microscope. Data concerning patient age, sex, presence of guttae, and ECD were recorded. The eyes were classified into four groups by slit lamp examination according to modified Stocker's classification[9]:

Stage 1: Guttata cornea without the stroma or the epithelium being affected

Stage 2: Permeation of corneal stroma with fluid, edema of epithelium, and bullae formation

Stage 3: Late stages with subepithelial connective tissue formation, vascularization, and scar formation

Other eyes without corneal guttae were classified as stage 0. During the rest of the article, the term Fuchs' corneal dystrophy (FCD) represents stage 2 and 3, since eyes in these stages have symptoms related to corneal edema. The study complied with the Declaration of Helsinki. Approval was granted by the Committee for the Protection of Human Subjects of each hospital.

Mathematical Model of Endothelial Cell Loss Rate

To construct a mathematical model of decrease in endothelial cells, we made the following two assumptions:

1. The ECD at 5 years of age is 3600 cells/mm^2. This is common to all classes.
2. From 5 years of age, the decrease rate (percent/year) of ECD is constant in each class, but different between classes.

Murphy et al.[10] reported that during first 2 years of life ECD decreased rapidly because of corneal growth, and after that the decrease rate slows down to 0.56%/year. The effect of corneal growth on ECD ends at 5 years of age or earlier. To simplify our mathematical model, we assumed that ECD at 5 years of age was common to all classes and regarded this point as the base point of age-ECD curve in our mathematical model. Because the onset of FCD is in adulthood, we believe that this assumption is acceptable. We substituted the mean ECD of normal 5-year-old children (3600 cells/mm^2) in the report of Nucci et al.[11] for the base point. We assumed that the (percentage) decrease rate is dependent on the class, and it is constant in each class from 5 years of age. Based on these assumptions, the following differential equation stands:

$$dE_{(t)}/d(t) = -(D/100) \cdot E_{(t)}$$

$$E_{(t=0)} = 3600$$

where t is age 5 years; $E_{(t)}$ is endothelial cell density at t years (in cells per square millimeter); and D is the decrease rate (percent).

The solution to the differential equation is the following:

$$E_{(t)} = 3600e^{[-(D/100)t]}$$

Using this mathematical model, an age-ECD curve in each class can be drawn by the least-squares method. An age-ECD curve of optimal decrease rate can be drawn as well.

Statistical Analysis

Scatterplotting, analysis of variance (ANOVA), nonparametric density smoothing, age-ECD curve, and other statistical analyses were calculated by or written in commercial software (Excel 2007; Microsoft, Redmond, WA, and JMP 8 software; SAS, Cary, NC). $P < 0.05$ was considered statistically significant.

Results

Characteristics of Patients

Age, sex, and stage of reviewed patients and eyes are presented in Table 1. The prevalence of guttata cornea (stage 1+2+3) was 12.73%. The prevalence of stage 1 was 10.65%, and FCD (stage 2+3) was 2.08%. The male: female ratio in each stage was as follows; 1: 1.03 (stage 0), 1: 1.88 (stage 1), 1: 2.43 (stage 2), and 1: 4.67 (stage 3). Females were more predisposed to stage 1 or FCD than males, and the ratio increased in advanced stages.

Age-ECD Curve of 2.0% Differentiates Fuchs' Dystrophy

Figure 1, left shows the scatterplot between age and ECD for each stage. Nonparametric density smoothing was drawn on the scatterplot (Fig. 1, right), which represents the contour of plot density. The age-ECD curves based on our mathematical model were drawn by the least-squares method. Table 2 shows ECD with sample sizes at 5-year intervals for grades 0 to 3, which enables the mean ECD data of grade 0 to 3 to be compared at various ages.

The decreased rate curve of stage 1 age-ECD was 0.81%, which was closer to that of stage 0 (decrease rate, 0.44%) than that of stage 2 (2.65%) or stage 3 (3.08%). The decrease rate of stage 0 in our study was 0.44%, which is within the range of

Table 1. The Age, Sex, and Stages of Reviewed Patients and Eyes

Patient Stage	Age, y (Mean ± SD)	Male (*n*)	Female (*n*)	Total (*n*)	Prevalence (%) Total	Male	Female
0	65.3 ± 16.2	848	872	1720			
1	68.5 ± 14.3	73	137	210	10.65	7.84	13.17
2	70.3 ± 10.6	7	17	24	1.22] 2.08	0.75] 1.07	1.63] 2.98
3	75.1 ± 12.4	3	14	17	0.86	0.32	1.35
Total	66.6 ± 15.4	931	1040	1971	12.73	8.91	16.15

Eye Stage	Male (*n*)	Female (*n*)	Total (*n*)
0	1426	1483	2909
1	103	205	308
2	13	28	41
3	5	18	23
Total	1547	1734	3281

Prevalence of FCD was calculated as sum of stage 2 and 3. In this table, if a patient had eyes in different stages, then he or she was classified in the severer of the stages between the eyes.

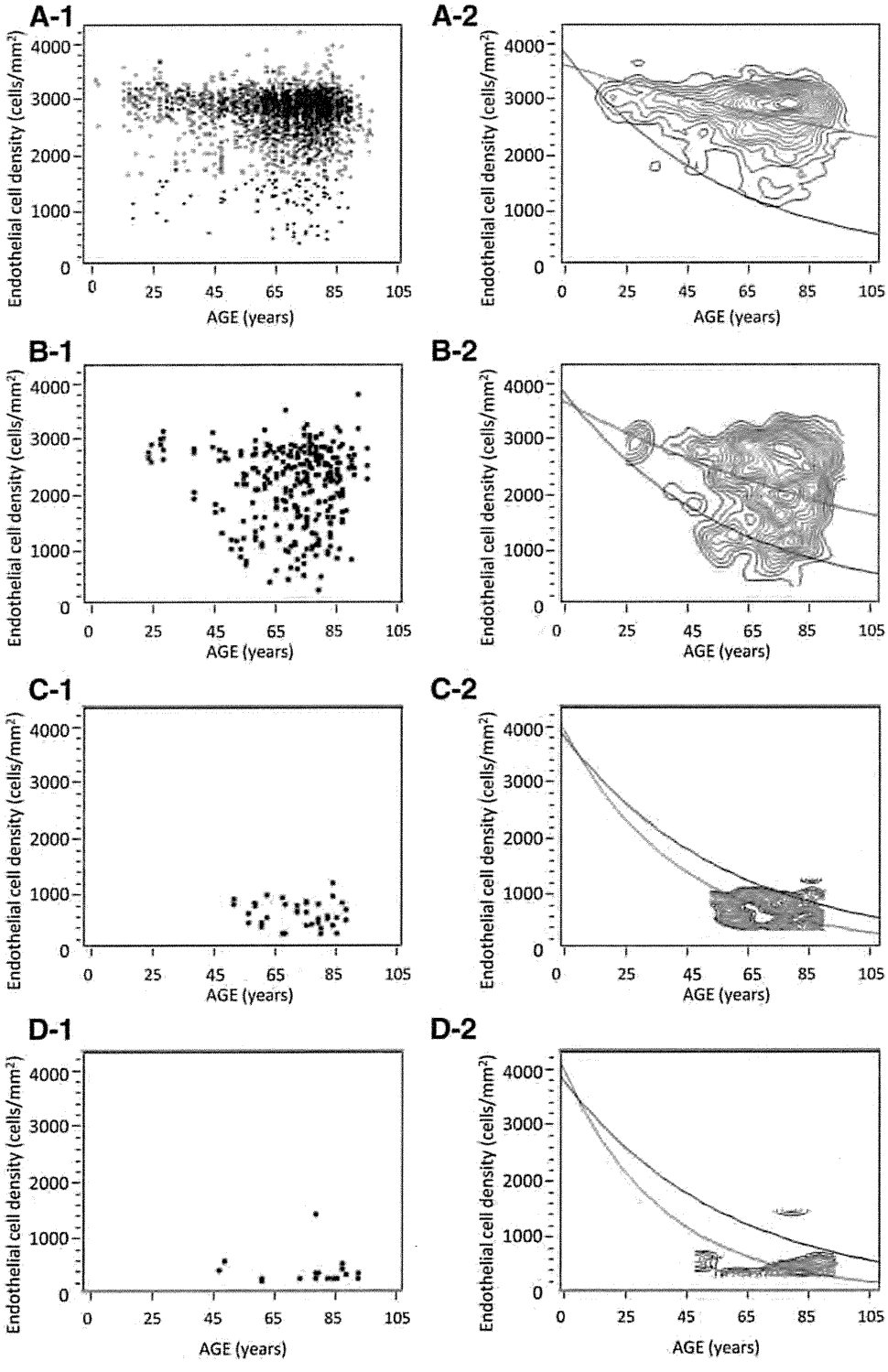

FIGURE 1. Scatterplots (*left*) and contour maps of nonparametric density smoothing (*right*) of each stage. (**A-1**, **A-2**) Stage 0, (**B-1**, **B-2**) stage 1, (**C-1**, **C-2**) stage 2, and (**D-1**, **D-2**) stage 3. *Red curves*: age-ECD curves of each stage calculated by least-squares method. The decrease rates of each stage were 0.44% (stage 0), 0.81% (stage 1), 2.65% (stage 2), and 3.08% (stage 3). The contour maps showed that the age-ECD curve of 2.00% decrease rate ($ECO_{2.0}$, *black curves*) ran through a trough between peaks of all stages. Most of the peaks in stages 0 and 1 were located above $ECO_{2.0}$, whereas peaks of stages 2 and 3 were located below $ECO_{2.0}$.

normal eyes reported in previous studies (Table 3).[10,12–16] Contour maps show that most of the peaks in stage 0 and 1 were located above the age-ECD curve of the 2.00% decrease rate, whereas peaks of stage 2 and 3 were located below this curve. Table 4 shows binary classification based on the age-ECD curve of a 2.00% decrease rate, designated novel ECD cutoff 2 ($ECO_{2.0}$), dividing stages 0+1 and stages 2+3 (Table 4) or stage 1 and stages 2+3 (Table 4). The high sensitivity and specificity of these classifications suggested that $ECO_{2.0}$ is an adequate cutoff between eyes with corneal edema and those without edema.

Age-ECD Curve of 1.4% and 2.0% Divides Stage 1 into Three Distinct Groups

The contour map of stage 1 consisted of several peaks. Figure 2 shows that the age-ECD curve of the 1.40% decrease rate, designated novel ECD-cutoff point 1 ($ECO_{1.4}$), divides these peaks into a high-density group ($>ECO_{1.4}$), and a low-density group ($<ECO_{1.4}$). ANOVA revealed that the age-ECD curves of each group predicted ECD according to age, with statistical significance: The *F* ratio and *P* value were 803.3 and <0.0001

TABLE 2. Mean ECD with Sample Sizes at 5-Year Intervals for Grades 0 to 3

	0–9 y		10–14 y		15–19 y		20–24 y		25–29 y	
	Eyes	**ECD**	**Eyes**	**ECD**	**Eyes**	**ECD**	**Eyes**	**ECD**	**Eyes**	**ECD**
Stage 0	4	3073.3 ± 392.6	7	3020.4 ± 330.1	47	2769.2 ± 530.1	31	2837.4 ± 567.3	60	2853.1 ± 507.6
Stage 1	0	—	0	—	0	—	4	2765.0 ± 128.8	6	2954.5 ± 175.6
Stage 2	0	—	0	—	0	—	0	—	0	—
Stage 3	0	—	0	—	0	—	0	—	0	—
	30–34 y		**35–39 y**		**40–44 y**		**45–49 y**		**50–54 y**	
	Eyes	**ECD**	**Eyes**	**ECD**	**Eyes**	**ECD**	**Eyes**	**ECD**	**Eyes**	**ECD**
Stage 0	58	2732.6 ± 511.3	54	2741.9 ± 324.7	80	2672.2 ± 462.5	99	2687.8 ± 507.8	128	2754.6 ± 370.5
Stage 1	0	—	4	2423.0 ± 474.1	7	2503.7 ± 541.9	7	1934.3 ± 763.9	14	1865.2 ± 703.0
Stage 2	0	—	0	—	0	—	2	881.0 ± 60.8	2	592.0 ± 120.2
Stage 3	0	—	0	—	1	461.0	1	622.0	0	—
	55–59 y		**60–64 y**		**65–69 y**		**70–74 y**		**75–79 y**	
	Eyes	**ECD**	**Eyes**	**ECD**	**Eyes**	**ECD**	**Eyes**	**ECD**	**Eyes**	**ECD**
Stage 0	195	2701.2 ± 408.1	325	2671.9 ± 464.4	384	2677.7 ± 449.1	494	2698.4 ± 435.0	496	2691.2 ± 421.3
Stage 1	25	2105.2 ± 673.3	28	2219.4 ± 695.5	39	2124.8 ± 743.7	61	2242.5 ± 719.4	44	2159.0 ± 741.7
Stage 2	4	645.8 ± 224.3	2	797.5 ± 282.1	7	562.9 ± 329.5	7	730.7 ± 149.5	7	483.0 ± 183.7
Stage 3	2	284.5 ± 21.9	0	—	0	—	2	302.5 ± 3.5	7	524.0 ± 418.9
	80–84 y		**85–89 y**		**≥90 y**					
	Eyes	**ECD**	**Eyes**	**ECD**	**Eyes**	**ECD**				
Stage 0	309	2698.9 ± 440.4	116	2624.5 ± 457.3	22	2563.7 ± 299.3				
Stage 1	47	2264.2 ± 556.2	17	2279.2 ± 597.9	5	2962.0 ± 597.1				
Stage 2	7	680.6 ± 318.1	3	723.3 ± 155.7	0	—				
Stage 3	5	302.4 ± 5.4	3	482.3 ± 97.1	2	352.5 ± 74.2				

Eye data are expressed as the number, and the ECD in cells per square millimeter.

in the high-density group and 945.7 and <0.0001 in the low-density group. The decrease rate of the age-ECD curve in the high-density group was 0.56%, which was very close to that of the stage 0 age-ECD curve. On the other hand, the decrease rate in the low-density group was 2.00%, which coincided with $ECO_{2.0}$. These results suggest that the decrease rate of the high-density group in stage 1 was nearly normal, whereas the low-density group in stage 1 was located on the border between eyes with and without corneal edema. We therefore classified stage 1 on the basis of $ECO_{1.4}$ and $ECO_{2.0}$, as follows (Fig. 3):

Stage 1a, asymptomatic guttata cornea (AGC): above $ECO_{1.4}$

Stage 1b, borderline guttata cornea (BGC): between $ECO_{1.4}$ and $ECO_{2.0}$

Stage 1c, preliminary stage of FCD (pre-FCD): below $ECO_{2.0}$

TABLE 3. Decrease Rates of Stage 0 in the Present Study and Normal Unoperated Eyes Reported in the Previous Studies

Author	Decrease Rate (%/y)	Nation
Murphy et al.[10]	0.56	United States
Cheng et al.[12]	1.00	England
Ambrose et al.[13]	0.60	England
Numa et al.[14]	0.30	Japan
Bourne et al.[15]	0.60	United States
Rao et al.[16]	0.30	India
Present study	0.44	Japan

DISCUSSION

To obtain a sufficient number of age-ECD data to compare FCD (stage 2+3), guttata cornea without edema (stage 1), and control group without guttata cornea (stage 0), we performed a retro-

TABLE 4. Binary Classification of Clinical Stage

Clinical Stage	Classification Based On $ECO_{2.0}$		
	Below $ECO_{2.0}$	**Above $ECO_{2.0}$**	**Total**
Total Eyes			
Stage 2+3	60	4	64
Stage 0+1	122	3095	3217
Total	182	3099	3281
Sensitivity, %	93.75		
Specificity, %	96.21		
Eyes with Guttata Cornea			
Stage 2+3	60	4	64
Stage 1	27	281	308
Total	87	285	372
Sensitivity, %	93.75		
Specificity, %	91.23		

Data are based on the age-ECD curve of 2.00% decrease rate as a novel ECD-cut-off ($ECO_{2.0}$), sensitivity and specificity to detect stage 2+3 from total eyes or the eyes with guttata cornea based on the classification.

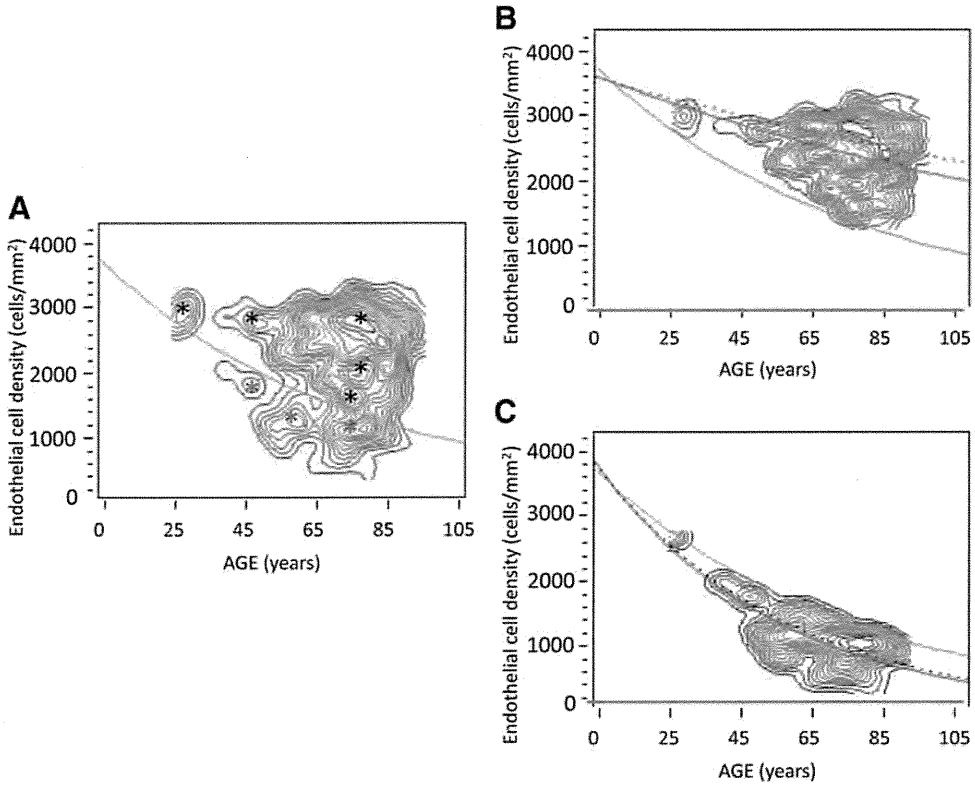

FIGURE 2. (**A**) The contour map of nonparametric density smoothing in stage 1. Stage 1 consisted of several peaks, and the age-ECD curve of 1.40% decrease rate ($ECO_{1.4}$, *green curve*) ran through a trough between peaks of high ECD group (*black asterisks*) and low ECD group (*red asterisks*). (**B**) High-density group in stage 1 above $ECO_{1.4}$. The age-ECD curve of this group (*red curve*) was close to that of stage 0 (*red dotted curve*), and the calculated decrease rate was 0.56%. (**C**) Low-density group in stage 1 below $ECO_{1.4}$. The age-ECD curve of this group (*red curve*) coincided with $ECO_{2.0}$ (*black dotted curve*), with a decrease rate of 2.00%.

spective, hospital-based review of total 1971 outpatients. In this study, we found a somewhat higher prevalence of guttata cornea than that found in previous reports in Japan. The prevalence of corneal guttae was reported to be 3.7% (1.5% in men, 5.5% in women) in Japan,[17,18] whereas it ranges from approximately 7% up to a remarkable 70.4% in North America, Iceland, and Europe.[1,8,19] In our study, the fact that subjects were hospital-based may have caused a higher prevalence. However, such bias does not have an effect on the validity of the mathematical model derived from the data. The following tendency of prevalence was apparent in our group of subjects: First, females were more predisposed to stages 1, 2, and 3 than were males, and the female ratio increased as stages progressed. Second, the prevalence of FCD was much smaller than stage 1. An increase in the female ratio in progressing stages suggested that sex may have some role not only in the onset but also the progression of the disease. Apparent difference of prevalence between FCD and stage 1 suggest the existence of a patient group in stage 1 that does not progress to corneal edema despite having guttata cornea.

Our model is based on the assumptions that the ECD at 5 years of age is common to all classes and that the decrease rate

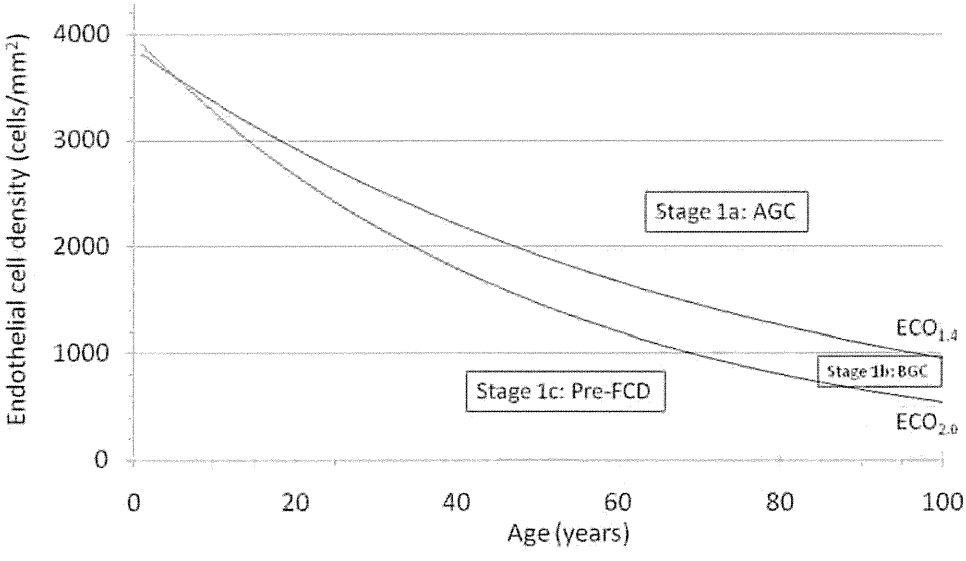

Age (years)		20	30	40	50	60	70	80	90
ECD (cells/mm²)	$ECO_{1.4}$	2918	2537	2205	1917	1667	1449	1260	1095
	$ECO_{2.0}$	2667	2184	1788	1464	1198	981	803	658

FIGURE 3. Proposed classification of eyes in stage 1 based on $ECO_{1.4}$ and $ECO_{2.0}$. Eyes in stage 1a above $ECO_{1.4}$ were named AGC, which had a decrease rate as low as stage 0. Eyes in stage 1c below $ECO_{2.0}$ had a decrease rate as high as FCD (stages 2 and 3), and therefore, this stage was named pre-FCD. Stage 1b between $ECO_{1.4}$ and $ECO_{2.0}$ was named BGC. The table below the graph shows the coordinates of $ECO_{1.4}$ and $ECO_{2.0}$.

of ECD percentage per year) is constant but with a different value of each class. The use of these assumptions may be a debatable point when discussing the validity of our study. However, the results of our mathematical model show ECD decrease rates that are acceptable when compared with clinical observations. The decrease rate of 0.44% in stage 0 is within the range of values of normal unoperated eyes reported in the previous studies.[10,12–16] Furthermore, since $ECO_{1.4}$ and $ECO_{2.0}$ runs through a clearly defined trough between peaks on the scatterplot, and $ECO_{2.0}$ divided stages 0+1 and stages 2+3 or stage 1 and stages 2+3 with high sensitivity and specificity, we believe our mathematical model for classifying patients with guttae based on ECD decrease rates is adequate for predicting the prognosis.

The $ECO_{1.4}$ and $ECO_{2.0}$ curves based on our mathematical model divided stage 1 into three subgroups, stage 1a, 1b, and 1c. The ECD decrease rate of stage 1a was close to that of stage 0, that is, almost normal. Schnitzer and Krachmer reported on 44 relatives of 12 families with guttata cornea which appeared normal on slit-lamp examination and endothelial cell parameters.[20] These eyes presumably belonged to stage 1a of our classification. In addition, because the distribution of patients of stage 1a was located above $ECO_{1.4}$, the risk of progressing to corneal edema may be as low as stage 0. If a patient was on the curve of a 1.4% decrease rate, the ECD would be 1095 cells/mm^2 even when he was 90 years old. Presumption of low risk of stage 1 is supported by analysis of variance, showing that age-ECD curves of each stage had significant predictability.

It was surprising that the age-ECD curve of the low-density group of stage 1 (stages 1b and 1c) coincided completely with $ECO_{2.0}$. The former was calculated by the least-squares method of the low-density group of stage 1, whereas the latter was obtained from trough between peaks of stages 0 to 3 on scatterplots. This result suggests that the low-density group of stage 1 was located on the border between stage 0 and FCD. Eyes in stage 1c below $ECO_{2.0}$ have a decrease rate as high as FCD, suggesting that these eyes have a risk to progress to FCD, even if there was no corneal edema present. This was the rationale for referring to stage 1c as pre-FCD. Further prospective study of patients in stage 1b and 1c is needed to determine whether stage 1c is a preliminary stage of FCD.

Recently, several pathogenic mechanisms, such as oxidative stress or unfolded protein response, have been reported as causes of FCD.[21,22] The difference in resistance against such stress may cause the difference in decrease rates between stages. Previous reports suggested that ECD of some eyes with guttata cornea did not decrease significantly compared with normal eyes after cataract surgery,[7,23] whereas some eyes in other reports showed a significantly higher decrease.[24] When we adapted data from these reports to our classification, we found that most of the former eyes with no difference in ECD (18/21 eyes) were categorized as stage 1a, suggesting that our classification may be used to identify patients with a higher risk of endothelial damage due to external stress. Future studies on guttata corneas using our classification may help clarify the mechanism of FCD progression.

In conclusion, we assessed distribution and endothelial loss rate of guttata cornea stages 0 to 3 and determined new cutoff curves $ECO_{1.4}$ and $ECO_{2.0}$ by using scatterplots. Our mathematical model is a simple method for predicting the prognosis of patients with guttata cornea.

References

1. Weisenthal RW, Streeten BW, eds. *Posterior Membrane Dystrophies.* London: Elsevier Mosby; 2005.
2. Edelhauser HF, Ubels JL, eds. *The Cornea and the Sclera.* 10th ed. ed. St. Louis: Mosby; 2003.
3. Al-Yousuf N, Mavrikakis I, Mavrikakis E, Daya SM. Penetrating keratoplasty: indications over a 10 year period. *Br J Ophthalmol.* 2004;88(8):998–1001.
4. Dobbins KR, Price FW Jr, Whitson WE. Trends in the indications for penetrating keratoplasty in the midwestern United States. *Cornea.* 2000;19(6):813–816.
5. Kang PC, Klintworth GK, Kim T, et al. Trends in the indications for penetrating keratoplasty. 1980–2001. *Cornea.* 2005;24(7):801–803.
6. Krachmer JH, Purcell JJ Jr, Young CW, Bucher KD. Corneal endothelial dystrophy: a study of 64 families. *Arch Ophthalmol.* 1978; 96(11):2036–2039.
7. Kitagawa K, Fujisawa A, Mizuno T, Sasaki K. Twenty-three cases of primary cornea guttata. *Jpn J Ophthalmol.* 2001;45(1):93–98.
8. Adamis AP, Filatov V, Tripathi BJ, Tripathi RC. Fuchs' endothelial dystrophy of the cornea. *Surv Ophthalmol.* 1993;38(2):149–168.
9. Stocker FW. The endothelium of the cornea and its clinical implications. *Trans Am Ophthalmol Soc.* 1953;51:669–786.
10. Murphy C, Alvarado J, Juster R, Maglio M. Prenatal and postnatal cellularity of the human corneal endothelium: a quantitative histologic study. *Invest Ophthalmol Vis Sci.* 1984;25(3):312–322.
11. Nucci P, Brancato R, Mets MB, Shevell SK. Normal endothelial cell density range in childhood. *Arch Ophthalmol.* 1990;108(2):247–248.
12. Cheng H, Jacobs PM, McPherson K, Noble MJ. Precision of cell density estimates and endothelial cell loss with age. *Arch Ophthalmol.* 1985;103(10):1478–1481.
13. Ambrose VM, Walters RF, Batterbury M, Spalton DJ, McGill JI. Long-term endothelial cell loss and breakdown of the blood-aqueous barrier in cataract surgery. *J Cataract Refract Surg.* 1991; 17(5):622–627.
14. Numa A, Nakamura J, Takashima M, Kani K. Long-term corneal endothelial changes after intraocular lens implantation: anterior vs posterior chamber lenses. *Jpn J Ophthalmol.* 1993;37(1):78–87.
15. Bourne WM, Nelson LR, Hodge DO. Central corneal endothelial cell changes over a ten-year period. *Invest Ophthalmol Vis Sci.* 1997;38(3):779–782.
16. Rao SK, Ranjan Sen P, Fogla R, Gangadharan S, Padmanabhan P, Badrinath SS. Corneal endothelial cell density and morphology in normal Indian eyes. *Cornea.* 2000;19(6):820–823.
17. Kitagawa K, Kojima M, Sasaki H, et al. Prevalence of primary cornea guttata and morphology of corneal endothelium in aging Japanese and Singaporean subjects. *Ophthalmic Res.* 2002;34(3): 135–138.
18. Nagaki Y, Hayasaka S, Kitagawa K, Yamamoto S. Primary cornea guttata in Japanese patients with cataract: specular microscopic observations. *Jpn J Ophthalmol.* 1996;40(4):520–525.
19. Zoega GM, Fujisawa A, Sasaki H, et al. Prevalence and risk factors for cornea guttata in the Reykjavik Eye Study. *Ophthalmology.* 2006 Apr;113(4):565–569.
20. Schnitzer JI, Krachmer JH. A specular microscopic study of families with endothelial dystrophy. *Br J Ophthalmol.* 1981;65(6): 396–400.
21. Buddi R, Lin B, Atilano SR, Zorapapel NC, Kenney MC, Brown DJ. Evidence of oxidative stress in human corneal diseases. *J Histochem Cytochem.* 2002;50(3):341–351.
22. Engler C, Kelliher C, Spitze AR, Speck CL, Eberhart CG, Jun AS. Unfolded protein response in Fuchs endothelial corneal dystrophy: a unifying pathogenic pathway? *Am J Ophthalmol.* 2010;149(2):194–202-e2.
23. Stur M, Grabner G, Dorda W. Changes of the corneal endothelium following intracapsular cataract extraction with implantation of semiflexible anterior chamber lenses. I. Results of the early postoperative period. *Acta Ophthalmol (Copenh).* 1984;62(4):586–594.
24. Bourne WM, Nelson LR, Hodge DO. Continued endothelial cell loss ten years after lens implantation. *Ophthalmology.* 1994; 101(6):1014–1022.

Cornea

Herpes Simplex Virus Type 1–Induced Transcriptional Networks of Corneal Endothelial Cells Indicate Antigen Presentation Function

Dai Miyazaki,[1] Tomoko Haruki,[1] Sachiko Takeda,[1] Shin-ichi Sasaki,[1] Keiko Yakura,[1] Yuki Terasaka,[1] Naoki Komatsu,[1] Satoru Yamagami,[2] Hirokazu Touge,[3] Chizu Touge,[1] and Yoshitsugu Inoue[1]

Purpose. To determine the transcriptional response of cultured human corneal endothelial (HCEn) cells after herpes simplex virus type (HSV-1) infection and to characterize the primary functional elements and antiviral responses.

Methods. Immortalized HCEn cells were infected with HSV-1, and the global transcriptional profile was determined. The transcriptional networks of HCEn cells were constructed, and the inflammatory network nodes were evaluated for induction of candidate inflammatory mediators by protein array analyses. HSV-1–specific allogeneic T cells isolated from HSV-1–infected donors were co-cultured with HSV-1–pulsed HCEn cells, and T cell activation was assessed for antigen-specific proliferation.

Results. HSV-1 infection induced a global transcriptional activation with 331 genes significantly up- or downregulated compared with mock-infected HCEn cells ($P < 0.01$; 4< or 0.25> threshold). Network analysis showed that the HSV-1–induced transcriptome was specifically associated with antigen presentation, interferon-related responses, and cellular development, and was characterized by NF-κB and extracellular signal–regulated kinase signaling pathways. The primary associated function in the transcriptome was antigen presentation. Protein array analysis identified significant elevation of genes related to antigen presentation: *IL-6*, *IP-10*, *HVEML*, and interferon-γ. In addition, inflammatory cytokines including IL-8, MCP-1, TIMP-1, RANTES, I-309, MIF, MCP-2, IL-10, and SDF-1, in descending order, were significantly elevated. Mixed lymphocyte reaction assays showed that HSV-1–pulsed HCEn cells stimulated antigen-specific proliferation of allogeneic T lymphocytes.

Conclusions. HCEn cells respond to HSV-1 infection by initiating antigen presentation–related inflammatory responses, and they may serve as antigen-presenting cells. (*Invest Ophthalmol Vis Sci.* 2011;52:4282–4293) DOI:10.1167/iovs.10-6911

From the Divisions of [1]Ophthalmology and Visual Science and [3]Medical Oncology and Respirology, Faculty of Medicine, Tottori University, Tottori, Japan; and the [2]Department of Ophthalmology, Tokyo Women's Medical University Medical Center East, Tokyo, Japan.

Supported by Grand-in-Aid 20592076 and 21592258 for Scientific Research from the Japanese Ministry of Education, Science, and Culture.

Submitted for publication November 18, 2010; revised March 20, 2011; accepted April 14, 2011.

Disclosure: **D. Miyazaki**, None; **T. Haruki**, None; **S. Takeda**, None; **S. Sasaki**, None; **K. Yakura**, None; **Y. Terasaka**, None; **N. Komatsu**, None; **S. Yamagami**, None; **H. Touge**, None; **C. Touge**, None; **Y. Inoue**, None

Corresponding author: Dai Miyazaki, Division of Ophthalmology and Visual Science, Tottori University Faculty of Medicine, 36-1 Nishi-cho, Yonago Tottori 683-8504, Japan; dm@grape.med.tottori-u.ac.jp.

Corneal endotheliitis is a progressive form of corneal endotheliopathy that is characterized by focal, linear, or diffuse corneal edema. It can lead to progressive endothelial cell loss and to endothelial dysfunction. Relevant to this study, an intracameral injection of herpes simplex virus (HSV)-1 can lead to corneal endotheliitis,[1] and molecular diagnostic methods have shown that HSV contributes to the pathogenesis of corneal endotheliitis.[2]

The most frequent HSV-associated diseases of the cornea are epithelial keratitis and stromal keratitis, although stromal keratitis is known to involve the corneal endothelial cells as well. In contrast, pure endotheliitis without stromal keratitis due to HSV-1 is rare. Generally, detailed evaluations of the endothelial cells after HSV infection cannot be made by slit lamp examination and specular microscopy because of corneal opacification.[3] However, Hillenaar et al.[3] found by in vivo confocal microscopy that 43% of patients with common HSV keratitis had characteristic signs of endotheliitis, including pseudoguttata, enlarged intercellular gaps, infiltration of inflammatory cells into the endothelium, loss of cell boundary, spotlike holes, and endothelial denudation. These alterations of the corneal endothelial cells were shown to be resolved after antiviral and -inflammatory treatment, but the density of the endothelial cells in the affected eye decreased by 10.3%/year.

Corneal endothelial cells are permissive to HSV infection, as shown in human corneal endothelial (HCEn) cells grown in vitro by Sugioka et al.[4] Of note, the HCEn cells had higher susceptibility to HSV-1 and produced more viral particles than the representative permissive CV-1 cell line. So, the question arises as to how HCEn cells resist HSV infection despite their inherent susceptibility to HSV-1 infection. One possible answer to this question is the immune-modulatory properties of HCEn cells.

Anterior chamber–associated immune deviation (ACAID) is a well-known mechanism of peripheral immune tolerance,[5] and HCEn cells appear to be an important player in this process. For example, HCEn cells inhibit the CD3-stimulated proliferation of effector T cells in a cell-contact–dependent manner using programmed cell death 1 ligand 1 (PD-L1).[6] The HCEn cells can also convert $CD8^+$ T cells into regulatory T cells through membrane-bound TGF-β.[7] Thus, HCEn cells have the ability to modulate immune responses; however, it is still not known whether HCEn cells possess antigen-presentation capabilities.

How corneal epithelial and endothelial cells respond to pathogens is an important unanswered question, as is how they respond globally to pathogens. To try to answer these questions in an earlier study, we used human corneal epithelial cells (HCEps), which are representative cells permissive to HSV-1, to characterize the global transcriptional responses of

Investigative Ophthalmology & Visual Science, June 2011, Vol. 52, No. 7

the HCEp cells to HSV-1 infection. Application of bioinformatic methods showed that HCEp cells responded to HSV-1 infection by initiating mitogen-activated protein kinase-related transcriptional events, and also enhanced the release of IL-6 which induced an array of inflammatory mediators.[8]

In the same way, determining how HCEn cells respond to HSV infection may provide important clues about the physiological functions and contribution of HCEn cells. We will show that the global responses of HCEn cells to HSV-1 are markedly different from HCEp cells and are preferentially set to antigen presentation. This antigen-presentation capability was confirmed by their ability to stimulate HSV-1–specific allogeneic T-lymphocyte responses.

Materials and Methods

Cells

The HCEn cell line was established by transduction with hTERT and the large T gene, as described.[9] Retroviral vectors, BABE-hygro-hTERT (for hTERT), and MFG-tsT-IRES-neo (for SV40 large T antigen), were used, as described in detail.[6,10] The HCEn cells were propagated to confluence on 6- or 96-well plates in DMEM (Dulbecco's modified Eagle's medium; Invitrogen-Gibco, Grand Island, NY) supplemented with 10% fetal bovine serum.

Virus

Confluent monolayers of Vero cells were infected with HSV-1 (KOS strain).[8] To analyze the transcriptome of HSV-1–infected HCEn cells, we used the HCEp transcriptome as a reference, as reported.[8] Purified virus stock was prepared as described.[8] After 1 hour of adsorption, the medium containing the virus was aspirated, and the monolayers were re-fed with fresh HSV-1–free media. At the maximum cytopathic effect, the media were discarded, and the cells with a small amount of remaining media were frozen, thawed, sonicated, and centrifuged at 3000 rpm for 10 minutes. The supernatant was overlaid onto a sucrose density gradient (10%–60% wt/vol) and centrifuged on a swing rotor (SW28; Beckman, Fullerton, CA) for 1 hour at 11,500 rpm. The resultant visible band at the lower part of the gradient which contained the HSV-1 was washed by centrifugation at 14,000 rpm for 90 minutes and resuspended in a small volume of serum-free DMEM. The sample was then aliquotted and stored at −80°C until use. The infectivity of the virus was determined by plaque titration assay and was typically 1×10^9 plaque forming units (PFU) per milliliter. To infect HCEn cells with HSV-1, the cells were adsorbed with sucrose-density, gradient-purified virus stock for 1 hour and re-fed with fresh medium.

Microarray Procedures

HSV-infected HCEn cells were transcriptionally analyzed using a whole human genome microarray (Agilent Technologies, Santa Clara, CA) corresponding to 41,000 human genes and transcripts. HCEn cells were infected with HSV-1 at a multiplicity of infection (MOI) of 1. Total RNA was isolated from the HSV-infected HCEn cells 12 hours postinfection (PI; RNeasy Mini Kit; Qiagen, Hilden, Germany), according to the manufacturer's instructions. Mock-infected HCEn cells were used as controls.

Cyanine-3 labeled cRNA was prepared from 0.25 μg of RNA (One-Color Low RNA Input Linear Amplification PLUS kit; Agilent). Fragmented cRNA was hybridized to the whole human genome oligo microarray (model G4112F, Agilent) using a hybridization kit (Gene Expression Hybridization, G2545A; Agilent) and scanned with a microarray scanner (model G2565BA; Agilent). The acquired data were bioinformatically analyzed (GeneSpring GX 10; Agilent), and the genes differentially up- or downregulated after HSV infection were extracted from the whole genome by using *t*-test.

Functional Analysis of Data Set

Functional analysis was used to identify the biological function and/or disease that was most significant to the data set (Ingenuity Pathway analysis 7.0; Ingenuity Systems, Redwood, CA, computer program based on the Ingenuity Pathway Knowledge Base; http://www.ingenuity.com/products/pathways_analysis.html). Genes from the data set that met the cutoff of fourfold difference ($P < 0.01$) and were associated with biological functions and/or diseases in the Ingenuity Pathway Knowledge Base were selected for the analysis. Fisher's exact test was used to calculate a P value determining the possibility that each biological function and/or disease assigned to that data set was due to chance alone.

Canonical Pathway Analyses of Data Set

Canonical pathway analyses were used to identify the pathways from the pathways analysis library of canonical pathways that were most significant to the data set. Genes from the data set that met the cutoff of fourfold difference ($P < 0.01$) and were associated with a canonical pathway in the pathway knowledge base were selected for the analyses. The significance of the association between the data set and the canonical pathway was measured in two ways: (1) a ratio of the number of genes from the data set that map to the pathway divided by the total number of genes that map to the canonical pathway, and (2) the use of Fischer's exact test to calculate a P-value determining the probability that the association between the genes in the dataset and the canonical pathway can be explained by chance alone.

Network Analysis of the HSV-1–Induced Transcriptome

The set of extracted genes was analyzed for transcriptional networks of molecular events using pathway analysis. The resulting networks were evaluated by the significance scores, which were expressed as the negative logarithm of the P value. The obtained score indicated the likelihood that the assembly of a set of focus genes in a network could be explained by random chance alone.

Real-time RT-PCR

Total RNA was isolated from the HSV-infected HCEn cells and reverse transcribed using (QuantiTect Reverse Transcription Kit; Qiagen), and the cDNAs were amplified and quantified (LightCycler; Roche, Mannheim, Germany, QuantiTect SYBR Green PCR kit). The sequences of the real-time PCR primer pairs were *IFN-α1*: forward 5′-GGAGTTTGATGGCAACCAGT-3′ and reverse 5′-CTCTCCTCCTGCATCACACA-3′; and glyceraldehyde-3-phosphate dehydrogenase (*GAPDH*): forward 5′-AGCCACATCGCTCAGACAC-3′ and reverse 5′- GCCCAATACGACCAAATCC-3′.

To ensure equal loading and amplification, all products were normalized to *GAPDH* transcript as an internal control.

Cytokine Array Analyses

To profile the inflammatory cytokine after HSV infection, supernatants were collected from HCEn cells 12 hours PI and assayed with a cytokine antibody array (Human Body Array; RayBiotech, Norcross, GA). This process determined the level of expression of 80 cytokines. The intensity of the chemiluminescence signals was digitized (LAS-1000plus with MultiGauge software ver. 2.0; Fujifilm, Tokyo, Japan).

T-Lymphocyte Proliferation Assay

T lymphocytes were prepared from peripheral blood mononuclear cells of human donors with histories of recurrent herpetic lesions by using negative selection with an immune magnetic beads–based isolation kit (IMag; BD Biosciences, Franklin Lakes, NJ). These cells were further negatively selected for $CD4^+$ T cells with an isolation kit (IMag). HCEn cells were seeded into 96-well plates, exposed to purified HSV-1 (KOS strain) for 1 hour, and treated with mitomycin C (Sigma-Aldrich, St. Louis, MO) at 4.5 hours PI. The HSV-primed HCEn

cells were co-cultured with isolated T cells for 3 days and pulsed with BrdU for 12 hours. The incorporation of BrdU was measured by chemiluminescence-based ELISA (Roche). Interferon-γ levels in the supernatant were measured with an ELISA kit, according to the manufacturer's instructions (eBioscience, San Diego, CA).

The procedures used conformed to Declaration of Helsinki. Informed consent was obtained from all the participants.

Statistical Analyses

Data are presented as the mean ± SEM. Statistical analyses were performed using *t*-tests or ANOVA as appropriate.

Results

Microarray Analysis of HSV-1–Infected Corneal Endothelial Cells

Viral infection usually induces an interferon response from the host; however, the interferon response is generally silenced by HSV-1 infection by its exploitation.[11] Therefore, we first tested whether the HSV-1 infection induced an interferon response of HCEn cells. Similar to the HCEp response,[8] the HCEn cells transcriptionally induced an interferon response that was detected at 12 hours PI and was higher at 24 hours. The expression of IFN-α1 relative to GAPDH was 73.4 ± 19.4 relative copies at an MOI of 1 of HSV-1 and 6.4 ± 0.5 relative copies for a mock infection ($P < 0.005$).

To determine the early global responses to HSV-1, we conducted a transcriptional profiling of HSV-1–infected HCEn cells by microarray analysis. We identified 8979 genes that were differentially expressed in HSV-1–infected at 12 hours PI at an MOI of 1 ($P < 0.01$). To extract sets of virus-responsive genes, we set a threshold of fourfold expression changes. This threshold resulted in the detection of 453 upregulated genes and 8 downregulated genes in the HSV-1–infected HCEn cells (Table 1). Thus, HSV-1 infection of HCEn cells globally activated transcriptional responses.

The upregulated genes at the highest ratio were *RAS*, dexamethasone-induced 1 (*RASD1*), δ-like 1 (*DLL1*), SRY-box 3 (*SOX3*), activity-regulated cytoskeleton-associated protein (*ARC*), thyroxine deiodinase type III (*DIO3*), indoleamine 2,3-dioxygenase 1 (*IDO1*), *FLJ00049*, and 10 kDa interferon-γ-induced protein (*IP-10*, *CXCL10*).

The downregulated genes at the highest ratio were chromosome 18 open reading frame 55 (*C18orf55*), EF-hand domain (C-terminal)–containing 2 (*EFHC2*), and arachidonate 5-lipoxygenase-activating protein (*ALOX5AP*), which is required for leukotriene synthesis with 5-lipoxygenase.

Network Analysis of Upregulated or Downregulated Genes in HSV-Infected Human Corneal Endothelial Cells

To obtain a global view of HSV infection–induced phenomena in the HCEn cells, 330 genes were extracted from the 461 genes (fourfold difference, $P < 0.01$) and were analyzed for signaling interactions using a systems biological approach.

Using the data set of 330 genes, functional analysis was used to reveal functional associations with the HCEn transcriptome. The highest significant association was detected for antigen presentation function, and as much as 23% of the data set was associated with this function (Table 2). This analysis was followed by determining significant associations with antimicrobial response function and cell-mediated immune response (data not shown).

We next applied canonical pathway analysis to the data set to reveal their relative associations with the pathways. The results shown in Table 3 showed that the HCEn transcriptome is heavily favored toward interferon signaling as the primary pathway. The second association was with the pattern recognition receptor pathway, which would recognize HSV. These associations were consistent with their function as antigen-presenting cells (APCs).

To obtain a global view of biological interactions in the data set, we applied network analysis using the data base (Pathways Knowledge Base; Ingenuity Systems) of known signaling networks. We successfully generated five major biological networks with their significance scores ($P < 10^{-30}$; Table 4, Fig. 1).

Network 1 provided the highest significance score ($P < 10^{-48}$) and was represented by interferons including *IL-29*, interferon regulatory transcription factors (*IRF*s), and interferon-responsive genes including absent in melanoma 2 (*AIM2*), interferon-induced proteins (*IFI*), melanoma differentiation associated protein-5 (*IFIH1*, *MDA5*), interferon-induced proteins with tetratricopeptide repeats (*IFIT*), interferon-stimulated protein, 15 kDa (*ISG15*), 2′-5′-oligoadenylate synthetase (*OAS*), radical *S*-adenosyl methionine domain–containing 2 (*RSAD2*), SP110 nuclear body protein (*SP110*), and signal transducer and activator of transcription 1 (*STAT1*) and *STAT2*.

Another category in network 1 was the recognition of dsRNA and related molecules. This network included Toll-like receptor (*TLR*) 3, DEAD box polypeptide 58 (*DDX58*, *RIG-1*), *IFIH1* (*MDA5*), RIG-I-like receptor LGP2 (*DHX58*), and *OAS*. Of these, *TLR3*, *DDX58* (*RIG-1*), and *MDA5* are representative sensors of dsRNA. In addition, tumor necrosis factor ligand superfamily member 9 (*TNFSF9*, *4-1BB-L*), which are crucial costimulatory molecules for antigen presentation to induce T lymphocyte proliferation, were found to be significantly associated with this network. Thus, network 1 was annotated as antigen presentation, antimicrobial responses, and cell-mediated immune responses. Activation of this network was calculated to be significantly associated with the NF-κB cascade.

Network 2, with the second highest significance score ($P < 10^{-40}$), was annotated as cellular development, hematologic system development and function, and hematopoiesis. This network was summarized to the extracellular signal-regulated kinase (*ERK*) cascade, and granulocyte colony-stimulating factor (*CSF3*). CXC chemokines receptor 4 (*CXCR4*), phospholipase C (*PLC*) gamma, and spleen tyrosine kinase (SYK)/ζ-associated protein (*ZAP*) served as crucial nodes.

Network 3 was annotated as cell-to-cell signaling and interaction, hematologic system development and function, and immune cell trafficking. This network included *CCL3* (*MIP-1α*), *CCL5* (*RANTES*), interleukin (IL)-12 (*IL12*, *IL-12*), and tumor necrosis factor (*TNF*) ligand family molecules, including TNF superfamily, member 13b (*TNFSF13B*, *BAFF*), TNF ligand superfamily member 10 (*TNFSF10*, *TRAIL*), and TNF receptor superfamily, member 1B (*TNFRSF1B*, *TNFR-2*).

Network 4 was another significant antigen-presentation, function-related network, which was annotated as antigen presentation, cell-mediated immune response, and humoral immune response. This network included antigen-presentation–related genes, Th1-related chemokines and cytokines, and interleukin 6 (*IL6*, *IL-6*), which will determine the type of T lymphocyte responses. Essential components of the antigen presentation machinery, including MHC molecules and transporter associated with antigen processing (*TAP1*), were found in this network. Herpes virus entry mediator-ligand (*TNFSF14*, *HVEML*) found in this network is a co-stimulatory factor for T cells to interact with APCs and acts as a receptor for HSV.

Network 5 was annotated as cellular growth and proliferation, embryonic development, and gene expression. In the context of antigen presentation, Class II Major Histocompatibility Complex and transactivator (*CIITA*), a master transcriptional regulator essential for class II expression, was located in this network. Network 5 was also characterized by nuclear

TABLE 1. Significantly Upregulated or Downregulated Genes of Human Corneal Endothelial Cells after HSV-1 Infection

GenBank ID*	Gene Symbol	Change	Regulation
NM_016084	*RASD1*	239.5	Up
NM_005618	*DLL1*	158.7	Up
NM_005634	*SOX3*	118.5	Up
NM_015193	*ARC*	99.3	Up
NM_001362	*DIO3*	77.9	Up
NM_002164	*IDO1*	62.3	Up
AK024457	*FLJ00049*	62.0	Up
NM_001565	*CXCL10*	54.1	Up
NM_138800	*TRIM43*	53.0	Up
ENST00000334770	*ENST00000334770*	53.0	Up
NM_080657	*RSAD2*	51.2	Up
NM_005409	*CXCL11*	50.7	Up
BC141819	*BC141819*	49.6	Up
NM_020975	*RET*	48.3	Up
NM_152677	*ZSCAN4*	47.8	Up
NM_002590	*PCDH8*	46.7	Up
NM_201589	*MAFA*	43.8	Up
THC2750782	*THC2750782*	40.9	Up
NM_002523	*NPTX2*	38.3	Up
NM_170672	*RASGRP3*	38.3	Up
NM_005382	*NEFM*	37.9	Up
NM_020358	*TRIM49*	37.7	Up
NM_002522	*NPTX1*	35.7	Up
NM_001005217	*FRG2*	34.8	Up
NM_052942	*GBP5*	32.2	Up
NM_003733	*OASL*	29.8	Up
NM_144614	*MBD3L2*	29.3	Up
NM_032855	*HSH2D*	29.1	Up
NM_001012276	*PRAMEF8*	28.6	Up
NM_004561	*OVOL1*	27.6	Up
NM_002776	*KLK10*	27.0	Up
NM_001485	*GBX2*	26.8	Up
NM_002416	*CXCL9*	26.6	Up
BC040902	*PRAMEF2*	26.4	Up
AW105154	*AW105154*	26.3	Up
NM_006573	*TNFSF13B*	26.3	Up
ENST00000273083	*GRIP2*	26.1	Up
NM_016323	*HERC5*	25.7	Up
XR_016154	*LOC642425*	25.3	Up
NM_016358	*IRX4*	24.8	Up
NM_001775	*CD38*	24.4	Up
NM_002196	*INSM1*	24.3	Up
NM_014310	*RASD2*	23.8	Up
NM_003004	*SECTM1*	23.6	Up
NM_006705	*GADD45G*	22.5	Up
NM_052941	*GBP4*	21.9	Up
NM_001040429	*PCDH17*	21.8	Up
NM_022454	*SOX17*	21.8	Up
NM_004833	*AIM2*	21.7	Up
NM_002507	*NGFR*	21.3	Up
NM_003956	*CH25H*	20.4	Up
NM_138456	*BATF2*	19.9	Up
NM_172374	*IL4I1*	19.6	Up
NM_003810	*TNFSF10*	19.5	Up
BG547557	*BG547557*	19.5	Up
NM_004789	*LHX2*	18.7	Up
NM_001080535	*LINCR*	18.4	Up
THC2651958	*THC2651958*	18.2	Up
NM_001712	*CEACAM1*	18.2	Up
NM_001547	*IFIT2*	18.0	Up
NM_016135	*ETV7*	17.9	Up
THC2559380	*THC2559380*	17.9	Up
NM_000517	*HBA2*	17.4	Up
NM_004304	*ALK*	17.0	Up
NM_205848	*SYT6*	16.9	Up
NM_002985	*CCL5*	16.9	Up
NM_022147	*RTP4*	16.8	Up
NM_152611	*C20orf75*	16.6	Up
NM_014314	*DDX58*	16.6	Up

(*continues*)

TABLE 1. (*continued*). Significantly Upregulated or Downregulated Genes of Human Corneal Endothelial Cells after HSV-1 Infection

GenBank ID*	Gene Symbol	Change	Regulation
NM_182597	*FLJ39575*	16.4	Up
NM_022168	*IFIH1*	16.3	Up
NM_017699	*SIDT1*	16.1	Up
AF007190	*AF007190*	15.6	Up
NM_002661	*PLCG2*	15.6	Up
NM_014383	*ZBTB32*	15.6	Up
NM_005623	*CCL8*	15.3	Up
NM_017878	*HRASLS2*	15.2	Up
NM_153456	*HS6ST3*	15.1	Up
NM_001103	*ACTN2*	14.8	Up
NM_002201	*ISG20*	14.7	Up
NM_007365	*PADI2*	14.3	Up
NM_006877	*GMPR*	14.3	Up
NM_001008540	*CXCR4*	14.1	Up
NM_021804	*ACE2*	14.0	Up
NM_000706	*AVPR1A*	13.3	Up
NM_002460	*IRF4*	13.1	Up
BC025340	*MGC39372*	13.0	Up
NM_033261	*ID2*	13.0	Up
NM_006158	*NEFL*	12.8	Up
NM_002010	*FGF9*	12.8	Up
NM_001549	*IFIT3*	12.8	Up
NM_002463	*MX2*	12.8	Up
AY831680	*AY831680*	12.6	Up
NM_175887	*PRR15*	12.5	Up
NM_018295	*TMEM140*	12.4	Up
BI910665	*BI910665*	12.4	Up
NM_004976	*KCNC1*	12.4	Up
NM_001548	*IFIT1*	12.3	Up
NM_020766	*PCDH19*	12.3	Up
NM_004848	*C1orf38*	12.2	Up
NM_203311	*CSAG3A*	12.0	Up
ENST00000292729	*USP41*	11.7	Up
BX110856	*BX110856*	11.6	Up
ENST00000301807	*LBA1*	11.5	Up
NM_004522	*KIF5C*	11.5	Up
NM_144583	*ATP6V1C2*	11.5	Up
NM_017414	*USP18*	11.4	Up
NM_014398	*LAMP3*	11.4	Up
NM_031917	*ANGPTL6*	11.2	Up
NM_002534	*OAS1*	11.2	Up
NM_018438	*FBXO6*	11.1	Up
NM_153357	*SLC16A11*	11.1	Up
NM_003885	*CDK5R1*	11.1	Up
NM_017654	*SAMD9*	11.1	Up
AW977362	*AW977362*	11.1	Up
NM_017805	*RASIP1*	11.0	Up
THC2657593	*THC2657593*	10.9	Up
NM_001729	*BTC*	10.6	Up
NM_005220	*DLX3*	10.5	Up
NM_001017403	*IGR6*	10.4	Up
NM_145288	*ZNF342*	10.4	Up
NM_000076	*CDKN1C*	10.3	Up
NM_005430	*WNT1*	9.9	Up
NM_024625	*ZC3HAV1*	9.9	Up
NM_002699	*POU3F1*	9.8	Up
ENST00000360954	*HS3ST3B1*	9.8	Up
NM_017554	*PARP14*	9.7	Up
AK023743	*FLJ31033*	9.6	Up
NM_003265	*TLR3*	9.5	Up
ENST00000302057	*IRX2*	9.5	Up
NM_016582	*SLC15A3*	9.5	Up
NM_019891	*ERO1LB*	9.4	Up
D00044	*CCL3*	9.4	Up
NM_004256	*SLC22A13*	9.4	Up
AF085913	*AF085913*	9.3	Up
NM_015900	*PLA1A*	9.2	Up
NM_006684	*CFHR4*	9.2	Up
BC029255	*BC029255*	9.2	Up

(*continues*)

TABLE 1. (*continued*). Significantly Upregulated or Downregulated Genes of Human Corneal Endothelial Cells after HSV-1 Infection

GenBank ID*	Gene Symbol	Change	Regulation
AB002384	*C6orf32*	9.2	Up
NM_024119	*IGP2*	9.2	Up
NM_004235	*KLF4*	9.2	Up
NM_152703	*SAMD9L*	9.1	Up
NM_004909	*CSAG2*	9.1	Up
AK074335	*NANP*	9.1	Up
NM_009587	*IGALS9*	9.0	Up
NM_014587	*SOX8*	9.0	Up
NM_004438	*EPHA4*	9.0	Up
NM_021096	*CACNA1I*	8.9	Up
NM_024490	*ATP10A*	8.9	Up
NM_003516	*HIST2H2AA3*	8.8	Up
NM_206827	*RASL11A*	8.7	Up
AK002042	*BET3L*	8.7	Up
NM_152309	*PIK3AP1*	8.6	Up
NM_005515	*HLXB9*	8.5	Up
NM_016569	*TBX3*	8.5	Up
NM_032206	*NLRC5*	8.5	Up
NM_144602	*C16orf78*	8.4	Up
NM_000775	*CYP2J2*	8.3	Up
NM_004165	*RRAD*	8.3	Up
NM_000246	*CIITA*	8.2	Up
NM_012193	*FZD4*	8.2	Up
NM_001080494	*C1orf34*	8.1	Up
AK125510	*C1orf104*	8.1	Up
NM_019055	*ROBO4*	8.0	Up
NM_004031	*IRF7*	7.9	Up
NM_001243	*TNFRSF8*	7.9	Up
AK074050	*MYO1G*	7.8	Up
NM_138433	*KLHDC7B*	7.8	Up
NM_013435	*RAX*	7.8	Up
NM_021065	*HIST1H2AD*	7.8	Up
AK091308	*AK091308*	7.7	Up
BM928667	*BM928667*	7.7	Up
NM_006186	*NR4A2*	7.7	Up
NM_014290	*TDRD7*	7.7	Up
NM_001007139	*IGF2*	7.6	Up
NM_138621	*BCL2L11*	7.6	Up
NM_178445	*CCRL1*	7.5	Up
NM_004673	*ANGPTL1*	7.5	Up
XM_211749	*LOC285047*	7.4	Up
AF086011	*AF086011*	7.4	Up
NM_021258	*IL22RA1*	7.4	Up
NM_004378	*CRABP1*	7.4	Up
BC093991	*HSPB9*	7.4	Up
AK095727	*AK095727*	7.3	Up
BC014346	*BC014346*	7.3	Up
NM_172140	*IL29*	7.3	Up
NM_000261	*MYOC*	7.3	Up
NM_002176	*IFNB1*	7.3	Up
NM_016817	*OAS2*	7.2	Up
NM_017639	*DCHS2*	7.2	Up
NM_002448	*MSX1*	7.2	Up
NM_173544	*FAM129C*	7.2	Up
NM_003655	*CBX4*	7.2	Up
ENST00000378953	*ENST00000378953*	7.1	Up
NM_207339	*PAGE2*	7.1	Up
NM_006914	*RORB*	7.1	Up
THC2526402	*THC2526402*	7.1	Up
NM_003328	*TXK*	7.0	Up
NM_153606	*FAM71A*	7.0	Up
NM_130467	*PAGE5*	7.0	Up
NM_020914	*RNF213*	7.0	Up
NM_002996	*CX3CL1*	7.0	Up
NM_198493	*ANKRD45*	7.0	Up
NM_004380	*CREBBP*	7.0	Up
NM_172109	*KCNQ2*	7.0	Up
NM_017523	*XAF1*	6.9	Up
NM_006144	*GZMA*	6.8	Up

(*continues*)

TABLE 1. (*continued*). Significantly Upregulated or Downregulated Genes of Human Corneal Endothelial Cells after HSV-1 Infection

GenBank ID*	Gene Symbol	Change	Regulation
AK091834	*FLJ34515*	6.8	Up
THC2474831	*THC2474831*	6.7	Up
NM_014817	*KIAA0644*	6.7	Up
NM_000758	*CSF2*	6.7	Up
NM_005853	*IRX5*	6.7	Up
NM_000558	*HBA1*	6.7	Up
NM_007332	*TRPA1*	6.7	Up
AI834280	*AI834280*	6.6	Up
AI028577	*AI028577*	6.6	Up
NM_003959	*HIP1R*	6.6	Up
NM_006228	*PNOC*	6.5	Up
NM_153479	*CSAG1*	6.5	Up
AK025221	*LOC441108*	6.5	Up
NM_002374	*MAP2*	6.5	Up
NM_015660	*GIMAP2*	6.5	Up
NM_020715	*PLEKHH1*	6.5	Up
ENST00000324559	*TMEM16E*	6.5	Up
ENST00000332844	*ENST00000332844*	6.4	Up
NM_000359	*TGM1*	6.4	Up
NM_172200	*IL15RA*	6.4	Up
NM_006820	*IFI44L*	6.4	Up
NM_003141	*TRIM21*	6.3	Up
NM_003811	*TNFSF9*	6.3	Up
NM_002147	*HOXB5*	6.3	Up
NM_007335	*DLEC1*	6.3	Up
AL117481	*DKFZP434B061*	6.3	Up
W91942	*W91942*	6.3	Up
BC073918	*BC073918*	6.2	Up
NM_000593	*TAP1*	6.2	Up
BC041467	*C17orf67*	6.2	Up
NM_006781	*C6orf10*	6.2	Up
NM_012465	*TLL2*	6.2	Up
NM_145641	*APOL3*	6.2	Up
NM_003807	*TNFSF14*	6.2	Up
NM_032727	*INA*	6.2	Up
NM_004364	*CEBPA*	6.1	Up
NM_021052	*HIST1H2AE*	6.1	Up
AK055279	*C8orf53*	6.1	Up
ENST00000269499	*ZCCHC2*	6.1	Up
ENST00000369158	*ENST00000369158*	6.1	Up
NM_021127	*PMAIP1*	6.1	Up
NM_005982	*SIX1*	6.0	Up
AV756170	*AV756170*	6.0	Up
NM_001040078	*LOC654346*	6.0	Up
NM_021822	*APOBEC3G*	5.9	Up
NM_013351	*TBX21*	5.9	Up
NM_005252	*FOS*	5.9	Up
DQ786194	*DQ786194*	5.9	Up
NM_004566	*PFKFB3*	5.9	Up
NM_006922	*SCN3A*	5.9	Up
THC2663297	*THC2663297*	5.9	Up
NM_004496	*FOXA1*	5.9	Up
NM_000683	*ADRA2C*	5.8	Up
NM_030641	*APOL6*	5.8	Up
NM_174896	*C1orf162*	5.8	Up
NM_012367	*OR2B6*	5.8	Up
NM_006074	*TRIM22*	5.8	Up
NM_057157	*CYP26A1*	5.8	Up
NM_002557	*OVGP1*	5.8	Up
ENST00000390253	*ENST00000390253*	5.8	Up
NM_017912	*HERC6*	5.8	Up
NM_014755	*SERTAD2*	5.7	Up
ENST00000377186	*ENST00000377186*	5.7	Up
NM_016642	*SPTBN5*	5.7	Up
NM_000759	*CSF3*	5.7	Up
NM_005533	*IFI35*	5.7	Up
ENST00000382595	*FAM90A9*	5.7	Up
NM_032265	*ZMYND15*	5.7	Up
NM_002468	*MYD88*	5.7	Up

(*continues*)

TABLE 1. (*continued*). Significantly Upregulated or Downregulated Genes of Human Corneal Endothelial Cells after HSV-1 Infection

GenBank ID*	Gene Symbol	Change	Regulation
NM_030930	*UNC93B1*	5.7	Up
NM_005170	*ASCL2*	5.6	Up
BQ213856	*BQ213856*	5.6	Up
NM_138819	*FAM122C*	5.6	Up
NM_006671	*SLC1A7*	5.6	Up
BC016934	*SOD2*	5.6	Up
THC2661318	*THC2661318*	5.6	Up
NM_170699	*GPBAR1*	5.6	Up
NM_003882	*WISP1*	5.6	Up
NM_004510	*SP110*	5.6	Up
NM_004585	*RARRES3*	5.5	Up
NM_019885	*CYP26B1*	5.5	Up
NM_005557	*KRT16*	5.5	Up
NM_006399	*BATF*	5.5	Up
NM_023940	*RASL11B*	5.5	Up
ENST00000303310	*ENST00000303310*	5.4	Up
AK125162	*AK125162*	5.4	Up
AA455656	*AA455656*	5.4	Up
NM_152431	*PIWIL4*	5.4	Up
ENST00000358378	*ENST00000358378*	5.4	Up
NM_003277	*CLDN5*	5.4	Up
NM_024783	*AGBL2*	5.3	Up
NM_002700	*POU4F3*	5.3	Up
NM_005980	*S100P*	5.3	Up
NM_031212	*SLC25A28*	5.3	Up
NM_006620	*HBS1L*	5.3	Up
NM_021035	*ZNFX1*	5.3	Up
NM_173042	*IL18BP*	5.3	Up
NM_033238	*PML*	5.2	Up
DB518505	*DB518505*	5.2	Up
NM_017709	*FAM46C*	5.2	Up
AF305819	*AF305819*	5.2	Up
NM_000161	*GCH1*	5.2	Up
NM_025079	*ZC3H12A*	5.2	Up
NM_019001	*XRN1*	5.2	Up
NM_020904	*PLEKHA4*	5.2	Up
NM_032784	*RSPO3*	5.1	Up
NM_153341	*IBRDC3*	5.1	Up
NM_153610	*CMYA5*	5.1	Up
NM_022750	*PARP12*	5.1	Up
NM_033292	*CASP1*	5.1	Up
BX109076	*BX109076*	5.1	Up
AK090515	*LOC283663*	5.1	Up
BC037791	*BC037791*	5.0	Up
NM_080552	*SLC32A1*	5.0	Up
NM_006187	*OAS3*	5.0	Up
AJ295982	*AJ295982*	5.0	Up
NM_025179	*PLXNA2*	5.0	Up
NM_033109	*PNPT1*	5.0	Up
NM_178140	*PDZD2*	5.0	Up
NM_005101	*ISG15*	5.0	Up
NM_017631	*FLJ20035*	5.0	Up
NM_021105	*PISCR1*	5.0	Up
NM_000070	*CAPN3*	5.0	Up
NM_052886	*MAL2*	5.0	Up
AK023773	*AK023773*	4.9	Up
AA573434	*AA573434*	4.9	Up
NM_033255	*EPSTI1*	4.9	Up
NM_001080391	*SP100*	4.9	Up
NM_203393	*LOC389458*	4.9	Up
NM_014850	*SRGAP3*	4.9	Up
AK021546	*AK021546*	4.9	Up
AK056817	*FLJ32255*	4.9	Up
NM_006576	*AVIL*	4.9	Up
AK056190	*DFNB31*	4.9	Up
ENST00000339446	*LOC387763*	4.9	Up
NM_002135	*NR4A1*	4.9	Up
NM_004688	*NMI*	4.9	Up
NM_002198	*IRF1*	4.9	Up
NM_000901	*NR3C2*	4.8	Up
AL117235	*PTCHD2*	4.8	Up
NM_001394	*DUSP4*	4.8	Up
NM_024956	*TMEM62*	4.8	Up
NM_003641	*IFITM1*	4.8	Up
NM_006095	*ATP8A1*	4.8	Up
NM_014080	*DUOX2*	4.8	Up
NM_138287	*DTX3L*	4.8	Up
THC2688196	*THC2688196*	4.8	Up
BI024548	*BI024548*	4.8	Up
NM_145019	*FAM124A*	4.8	Up
NM_006417	*IFI44*	4.8	Up
AK127223	*LOC284296*	4.7	Up
NM_006869	*CENTA1*	4.7	Up
NM_005248	*FGR*	4.7	Up
NM_002462	*MX1*	4.7	Up
NM_002286	*LAG3*	4.7	Up
BC010906	*MED9*	4.7	Up
NM_152612	*CCDC116*	4.7	Up
BU561469	*BU561469*	4.7	Up
NM_203446	*SYNJ1*	4.7	Up
NM_006624	*SLC34A2*	4.7	Up
NM_025195	*TRIB1*	4.7	Up
NM_002218	*ITIH4*	4.7	Up
NM_030766	*BCL2L14*	4.7	Up
NM_024778	*LONRF3*	4.7	Up
NM_021784	*FOXA2*	4.6	Up
AK027294	*AK027294*	4.6	Up
NM_175839	*SMOX*	4.6	Up
NM_006290	*TNFAIP3*	4.6	Up
BC013171	*BC013171*	4.6	Up
BC031266	*TRIM69*	4.6	Up
NM_015907	*LAP3*	4.6	Up
NM_005419	*STAT2*	4.6	Up
BC031319	*BC031319*	4.6	Up
NM_001066	*TNFRSF1B*	4.6	Up
THC2673062	*THC2673062*	4.6	Up
THC2513333	*THC2513333*	4.5	Up
NM_145053	*UBQLNL*	4.5	Up
NM_018381	*FLJ11286*	4.5	Up
NM_175065	*HIST2H2AB*	4.5	Up
NM_000600	*IL6*	4.5	Up
NM_024913	*FLJ21986*	4.5	Up
NM_019102	*HOXA5*	4.5	Up
NM_017539	*DNAH3*	4.5	Up
AK094730	*LOC283454*	4.5	Up
NM_173086	*KRT6C*	4.5	Up
NM_012420	*IFIT5*	4.5	Up
NM_002053	*GBP1*	4.5	Up
XR_017251	*LOC389386*	4.4	Up
BC014971	*BC014971*	4.4	Up
BC035583	*KIAA0999*	4.4	Up
NM_080829	*C20orf175*	4.4	Up
BC008632	*C6orf176*	4.4	Up
NM_198183	*UBE2L6*	4.4	Up
NM_139266	*STAT1*	4.4	Up
NM_014400	*LYPD3*	4.4	Up
NM_000307	*POU3F4*	4.4	Up
NM_178516	*EXOC3L*	4.4	Up
NM_145637	*APOL2*	4.4	Up
NM_004821	*HAND1*	4.4	Up
NM_173490	*TMEM171*	4.4	Up
NM_002089	*CXCL2*	4.4	Up
NM_138422	*LOC113179*	4.4	Up
NM_006018	*GPR109B*	4.3	Up
NM_173198	*NR4A3*	4.3	Up
ENST00000367675	*ENST00000367675*	4.3	Up
NM_018964	*SLC37A1*	4.3	Up
ENST00000319902	*KIAA1618*	4.3	Up

(*continues*)